



THE UNIVERSITY *of* EDINBURGH

## Edinburgh Research Explorer

### **Dual functionality of TiO<sub>2</sub>/biochar hybrid materials: photocatalytic phenol degradation in liquid phase and selective oxidation of methanol in gas phase**

**Citation for published version:**

Lisowski, P, Colmenares, JC, Masek, O, Lisowski, W, Lisovytskiy, D, Kamińska, A & Łomot, D 2017, 'Dual functionality of TiO<sub>2</sub>/biochar hybrid materials: photocatalytic phenol degradation in liquid phase and selective oxidation of methanol in gas phase', *ACS Sustainable Chemistry & Engineering*.  
<https://doi.org/10.1021/acssuschemeng.7b01251>

**Digital Object Identifier (DOI):**

[10.1021/acssuschemeng.7b01251](https://doi.org/10.1021/acssuschemeng.7b01251)

**Link:**

[Link to publication record in Edinburgh Research Explorer](#)

**Document Version:**

Peer reviewed version

**Published In:**

ACS Sustainable Chemistry & Engineering

**General rights**

Copyright for the publications made accessible via the Edinburgh Research Explorer is retained by the author(s) and / or other copyright owners and it is a condition of accessing these publications that users recognise and abide by the legal requirements associated with these rights.

**Take down policy**

The University of Edinburgh has made every reasonable effort to ensure that Edinburgh Research Explorer content complies with UK legislation. If you believe that the public display of this file breaches copyright please contact [openaccess@ed.ac.uk](mailto:openaccess@ed.ac.uk) providing details, and we will remove access to the work immediately and investigate your claim.



## **Dual functionality of TiO<sub>2</sub>/biochar hybrid materials: photocatalytic phenol degradation in liquid phase and selective oxidation of methanol in gas phase**

Paweł Lisowski<sup>a</sup>, Juan Carlos Colmenares<sup>a</sup>, Ondřej Mašek<sup>b</sup>, Wojciech Lisowski<sup>a</sup>, Dmytro Lisovytskiy<sup>a</sup>, Agnieszka Kamińska<sup>a</sup>, Dariusz Łomot<sup>a</sup>

<sup>a</sup> Institute of Physical Chemistry, Polish Academy of Sciences, Kasprzaka 44/52, 01-224 Warsaw, Poland

<sup>b</sup> UK Biochar Research Centre, School of Geosciences, University of Edinburgh, Edinburgh, UK, (UKBRC)

Corresponding Authors

E-mail: [plisowski@ichf.edu.pl](mailto:plisowski@ichf.edu.pl), [jcarloscolmenares@ichf.edu.pl](mailto:jcarloscolmenares@ichf.edu.pl)

### **Abstract**

A series of new inorganic-organic hybrid materials based on TiO<sub>2</sub> and new biochar-based supports (biochar obtained by pyrolysis of Miscanthus Straw Pellets (MSP) and Soft Wood Pellets (SWP) at 550 and 700 °C) were successfully prepared using ultrasound-assisted methodology. The resulting composites were characterized by a wide range physicochemical techniques and investigated in water and gas phase photocatalytic test reaction. Our best composite (TiO<sub>2</sub>/SWP700) achieved phenol degradation of 64.1% (under UV light) and 33.6% (under visible light). In addition, it also showed an extraordinarily high activity (~90 %) in selective oxidation of methanol to methyl formate in flow gas phase, high selectivity to methyl formate (~80 %) and high yield of methyl formate (~88 %) after 240 minutes of illumination. It can be noticed that when TiO<sub>2</sub> is supported on biochar, presented a superior photocatalytic ability and could be recycled at least 5 times in both photocatalytic runs tests with reproducible high photocatalytic efficiency.

**Keywords:** Biochar; TiO<sub>2</sub>; Synthesis of composite photocatalysts; Sonication for composite preparation; Phenol degradation; Methanol oxidation.

## Introduction

Photocatalytic technology offering low cost, high reactivity and easy recovery is of great relevance and significance for energy efficiency and environmental remediation. In recent years, TiO<sub>2</sub> has been extensively studied as an eminent material for its wide applications in photocatalysis due to its outstanding photocatalytic activity, low cost, extraordinary stability with minimum photocorrosion and so on.<sup>1-2</sup> Combining TiO<sub>2</sub> with non-toxic and abundant carbon materials have been employed in the study of novel possibilities for the design of photocatalysts which can show stable performance for heterogeneous photocatalysis.<sup>1-4</sup>

Recently, the great application potential of biochar from pyrolysis of biomass has received increasing attention, and there is a growing awareness of biochar's ability to provide a versatile and efficient platform for the synthesis of functionalized carbon materials.<sup>5-6</sup> Biochar can be defined as a porous solid rich by-product of thermal decomposition of wastes for non-fuel uses.<sup>7-8</sup> An important advantage of biochar over more conventional activated carbon is the presence surface functional groups (e.g. phenolic hydroxyl, carbonyl and carboxyl groups) on the surface of biochar.<sup>7-10</sup> Worth mentioning is the work by Matos<sup>10</sup> on the preparation of biochar-based functional materials and investigation a wide spectrum of harmful compounds in water and air under visible light irradiation.

Purification of water and air may be problematic with global relevance and heterogeneous photocatalysis has attracted considerable attention as a potential technique for pollution remediation. In this study we selected methanol and phenol as target compounds for photocatalytic treatment. Methanol was specified by The United States Environmental Protection Agency (U.S. EPA) as an important pollutant which may have significant negative impacts on natural environments.<sup>11-12</sup> Phenol is on the U.S. EPA's list of priority pollutants and potential for causing different effects on human health.<sup>13-14</sup>

Recent years have witnessed a rapid preparation of highly potent photoactive materials using ultrasound-based procedures which offer a facile, versatile synthetic tool and have great potential for the future of photocatalysts preparation.<sup>15-16</sup> Ultrasound-based procedures ensure extremely high localized pressures and temperatures in liquid phase reactions owing to cavitation effect which enhance the chemical reactivity.<sup>15-16</sup>

Based on the above considerations, a series of new inorganic-organic hybrid materials based on TiO<sub>2</sub> and new biochar-based supports were successfully prepared using ultrasound-

assisted wet impregnation method.<sup>17</sup> The photocatalytic activity and selectivity of prepared composites were performed using our reaction system for selective oxidation of methanol in gas phase and phenol photodegradation in liquid phase. To the best of our knowledge, this is the first complete work on photocatalytic oxidation of methanol in gas phase to form methyl formate and photocatalytic degradation of phenol by using biochar's modified on its surface with TiO<sub>2</sub> prepared by ultrasound-promoted wet impregnation methodology. The use of such non-conventional procedures for materials synthesis is very attractive from the perspective of green chemistry as it reduces costs and energy consumption.<sup>15-16</sup>

## Experimental section

### Preparation of biochar by pilot-scale continuous pyrolysis

The biochar's used as TiO<sub>2</sub> support in this study belong to the so called Edinburgh Standard Biochar set ([www.biochar.ac.uk/standard](http://www.biochar.ac.uk/standard)) and were produced using the UKBRC Stage III Pyrolysis Unit (rotary kiln pyrolyser) at the University of Edinburgh, shown in Figure 1. The rotary kiln pyrolysis unit consists of a biomass feeder, sealed rotating drum (ID = 0.244m, heated length 2.8m) heated by a set of electric heaters arranged in three heater banks of 16.67 kW each, a char handling screw conveyor, a collection vessel and an afterburner chamber. The unit can operate at temperatures of up to 850 °C, and achieve mean residence times of solids between few minutes to over 40 minutes. The chars used in this work were produced from softwood pellets (SWP) and miscanthus straw pellets (MSP) at peak pyrolysis temperature of 550 °C and 700 °C, and residence time at peak temperature of around 5 minutes. Table S1 (see Supplementary Information) contains basic characteristics of the four standard biochar used.

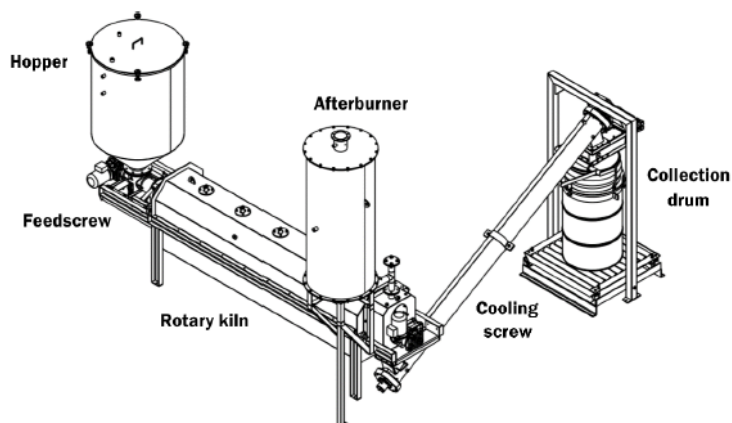


Figure 1. Rotary kiln pilot-scale pyrolysis unit (Stage III) at the UKBRC, University of Edinburgh (source: Anzac Ltd.)

### Preparation of hybrid TiO<sub>2</sub>-based biochar materials

Prior to the synthesis, biochar materials were washed thoroughly three times in boiling Milli-Q water and subsequently oven drying (110 °C). After optimizing the TiO<sub>2</sub> loading (15 wt. %, 25 wt. %, 35 wt. %) it can be stated that 25 wt. % loading of TiO<sub>2</sub> on biochar gave optimal performance, and therefore this loading level was used in preparation of all four biochar-supported TiO<sub>2</sub> catalysts in this study, as shown in Fig. 2. TiO<sub>2</sub>-based biochar materials biochar were prepared following the ultrasound-based procedures (surfactant-free synthesis) as previously shown in.<sup>17</sup> In brief, 500 mg of biochar was placed into a solution of Titanium (IV) isopropoxide (TTIP) (0.47 mL; 1.5 mmol) in 2-Propanol (total volume ratio of TTIP: 2-Propanol was 1:40) and the whole mixture was sonicated for 1 h (ultrasonic bath, frequency 35 kHz, 560 W, Sonorex Digitec-RC, Bandelin). The solvent was removed using a rotary vacuum evaporator assisted by sonication. The powder material was further dried for 3 h at 110 °C and subsequently after drying was calcined in a furnace at 400 °C at heating rate of 3 °C min<sup>-1</sup> for 5 h in an oxygen-deficient atmosphere (static air). The final samples were denoted as TiO<sub>2</sub>/MSP550, TiO<sub>2</sub>/MSP700, TiO<sub>2</sub>/SWP550 and TiO<sub>2</sub>/SWP700, where the second part indicates the type of biochar support used. For comparative purposes, TiO<sub>2</sub>/NORIT (NORIT, commercially available activated carbon) was prepared by ultrasound-assisted wet impregnation and TiO<sub>2</sub>/SWP700 was prepared without ultrasound.

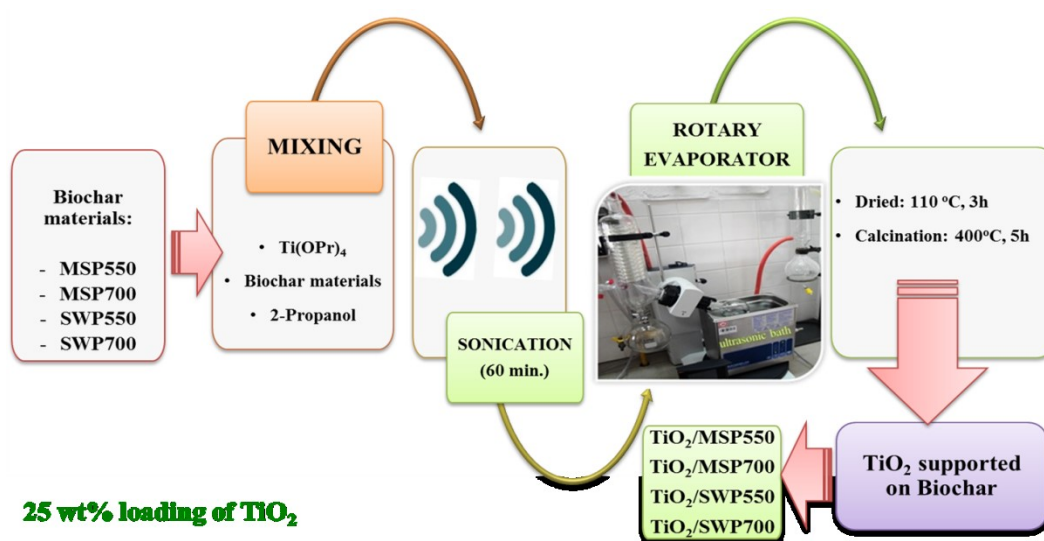


Figure 2. Synthesis procedure for hybrid TiO<sub>2</sub>/Biochar materials using ultrasound-based procedures.<sup>17</sup>

## Results and discussion

Textural properties of the prepared materials are summarized in Table S2 (see Supplementary Information), including the specific surface area and pore analysis. It was noted that the BET specific surface area of the TiO<sub>2</sub>/biochar materials increased compared to untreated biochar. Comparing the specific surface area of pure biochar materials like SWP550 and SWP700 (107 and 254 m<sup>2</sup> g<sup>-1</sup>, respectively), it should be noted that the most significant increase in the BET area is for TiO<sub>2</sub>/SWP550 and TiO<sub>2</sub>/SWP700 (400 and 399 m<sup>2</sup> g<sup>-1</sup> respectively) in comparison with other photocatalysts with the same TiO<sub>2</sub> content. As displayed in Fig. S1 (see Supplementary Information), the nitrogen adsorption–desorption isotherm of TiO<sub>2</sub>/MSP550, TiO<sub>2</sub>/MSP700 and TiO<sub>2</sub>/SWP550 indicate the presence of slit-shaped pores<sup>18-19</sup> associated with plate-like particles which is characteristic for microporous carbon materials. According to IUPAC classification, TiO<sub>2</sub>/SWP700 exhibits the four types of H4-hysteresis loops, pointing out that the prepared composite has mesoporous structure<sup>20</sup> with plate-like particles which usually give rise to narrow slit-shaped pores. Toward a better understanding the influence of ultrasound, TiO<sub>2</sub>/SWP700 without ultrasound was prepared. Results indicated that 65 % of BET surface area increase, together with rise in External BET in relation to TiO<sub>2</sub>/SWP700 prepared by ultrasound-assisted wet impregnation method compared to TiO<sub>2</sub>/SWP700 prepared by wet impregnation method (without ultrasound). It's worthy of note that the results obtained by ultrasound-assisted wet impregnation method showed a significant effect of sonication on textural properties. Based on these findings, it is likely that the larger external surface area, e.g., in case of TiO<sub>2</sub>/SWP700, would provide more opportunities for interaction of reactants with active sites of the photocatalyst and thus lead to greater activities. Additionally, higher BET of prepared materials may be ascribed to the effect of ultrasonic irradiation because it can produce cracks and increase mesoporous structure of the TiO<sub>2</sub>/SWP700. In addition, it can also result in formation of more photocatalytic surface-active centers and sites and thus is favorable to the improvement of the photocatalytic performance. This is owing to both, a larger number of photocatalytic surface-active centers and adsorption sites for compounds, and the increase of the ease reactants' transport through the network of interconnected pores. The plate-like particle structures are considered to be beneficial in utilizing more light and effective separation of photogenerated charge.<sup>18-19</sup>

The morphology and microstructure of prepared TiO<sub>2</sub>/biochar were investigated with SEM as revealed in Fig. 3. The images show irregular plate-like structure, which may be favorable for adsorption and photoreactions. Therefore, good organic contaminants adsorption

performance can be expected. Furthermore, obvious pores resulting from the slits among the plate-like particles can be also observed (observations also corroborated by BET characterization).

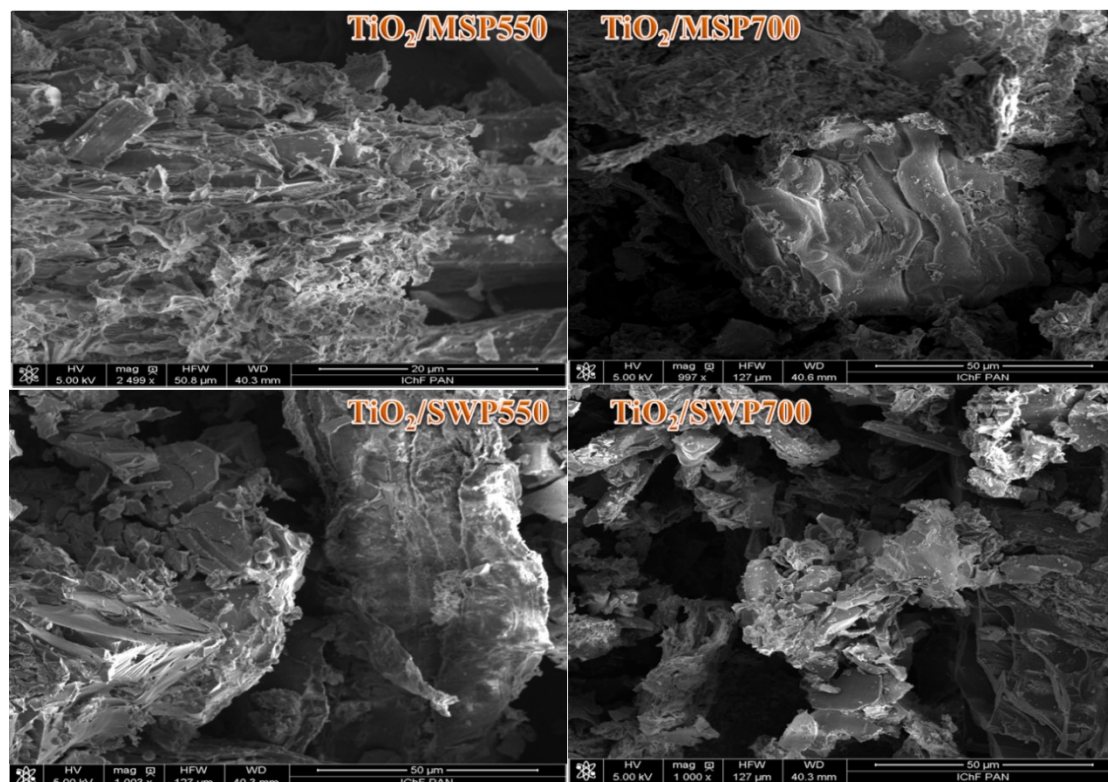


Figure 3. SEM images of TiO<sub>2</sub>/Biochar materials

X-ray Powder Diffraction (XRD) techniques were carried out in order to evaluate the structural characteristics of TiO<sub>2</sub>/Biochar materials. XRD patterns compiled in Fig. 4 pointed out the clear presence of a distinctive anatase phase in all TiO<sub>2</sub>-based biochar materials (Table 1). It is also worth noting that the existence a sharp peak at 26.6° in the case of TiO<sub>2</sub>/MSP700 corresponding to SiO<sub>2</sub>-quartz reflection. All materials exhibited almost identical XRD patterns differing only in terms of the intensity of the anatase diffraction lines. Some researchers claim that TiO<sub>2</sub> anatase phase exhibits lower rates of recombination e<sup>-</sup>/h<sup>+</sup> and higher adsorptive affinity for organic compounds compared to TiO<sub>2</sub> rutile phase.<sup>3, 5, 7</sup> In order to check the role of ultrasound, TiO<sub>2</sub>/SWP700 “in silence” was prepared (Table 1). Surprisingly, thus prepared material has different crystallite size (18 nm) than TiO<sub>2</sub>/SWP700 prepared by ultrasound-assisted wet impregnation method (22 nm). The cause for such differences may be owing to the intimate contact of two phases through a heterostructure vicinity. This new discovery may help to understand the roles of ultrasound in the formation of this kind of materials with photocatalytic properties.

Table 1. Results of crystallite size, crystal phase, band gap energy and absorption threshold over all tested photocatalysts.

Photocatalyst	XRD		UV-Vis	
	Crystallite size (nm)	Crystal phase	$E_{\text{gap}}$ (eV)	Absorption threshold (nm)
TiO <sub>2</sub> /MSP550	18	Anatase	2.43	515
TiO <sub>2</sub> /MSP700	23	Anatase	2.50	498
TiO <sub>2</sub> /SWP550	12	Anatase	2.45	508
TiO <sub>2</sub> /SWP700	22	Anatase	2.12	586
TiO <sub>2</sub> /SWP700_Without_US	18	Anatase	2.74	455

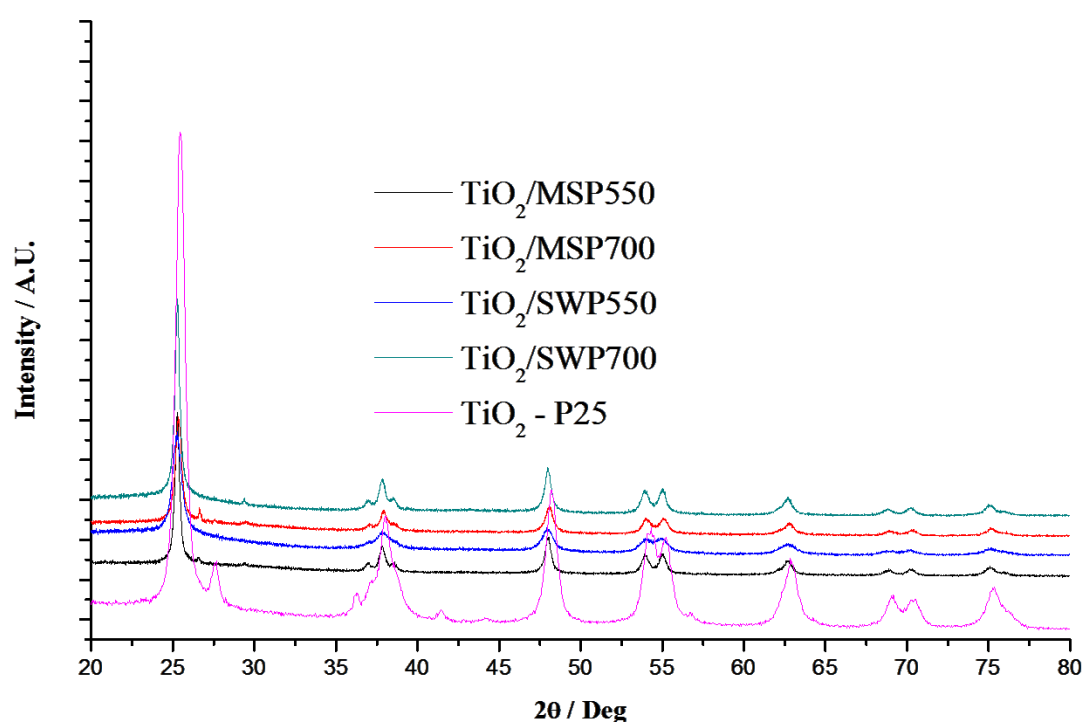


Figure 4. X-ray diffraction (XRD) patterns for TiO<sub>2</sub>/Biochar materials

XRF technique is a powerful tool for chemical analyses of many major and trace elements in prepared photocatalysts. It sometimes happens that trace elements (fingerprints) were observed in the elemental maps e.g. Rh, Fe, Cu from the X-ray source scatter. Additionally, it has been shown by XRF technique that main elements for biochar-based photocatalysts (results not shown) are Ti (~97 %) and Ca (1.3 ÷ 3.1%). In the case of TiO<sub>2</sub>/MSP550 and TiO<sub>2</sub>/MSP700 we also detected potassium (5.6 % and 7.6% respectively) and silicon (14 % and 8.8 % respectively).



To calculate the band gap energy, revealing the light harvesting ability of the resultant biochar-supported catalysts, the samples were subjected to UV–vis diffuse reflectance spectroscopy measurements (Fig. 5). The absorption edge is found to shift towards longer wavelengths was observed for TiO<sub>2</sub>/biochar photocatalysts (Table 1). On the other hand, TiO<sub>2</sub> P25 Evonik showed clear absorption edge at around 388 nm corresponding to a band gap of ~ 3.20 eV. The Kubelka-Munk function was developed to calculate band gap for TiO<sub>2</sub>/MSP550, TiO<sub>2</sub>/MSP700, TiO<sub>2</sub>/SWP550 and TiO<sub>2</sub>/SWP700 were found to be 2.43, 2.50, 2.45 and 2.12 respectively (Table 1).

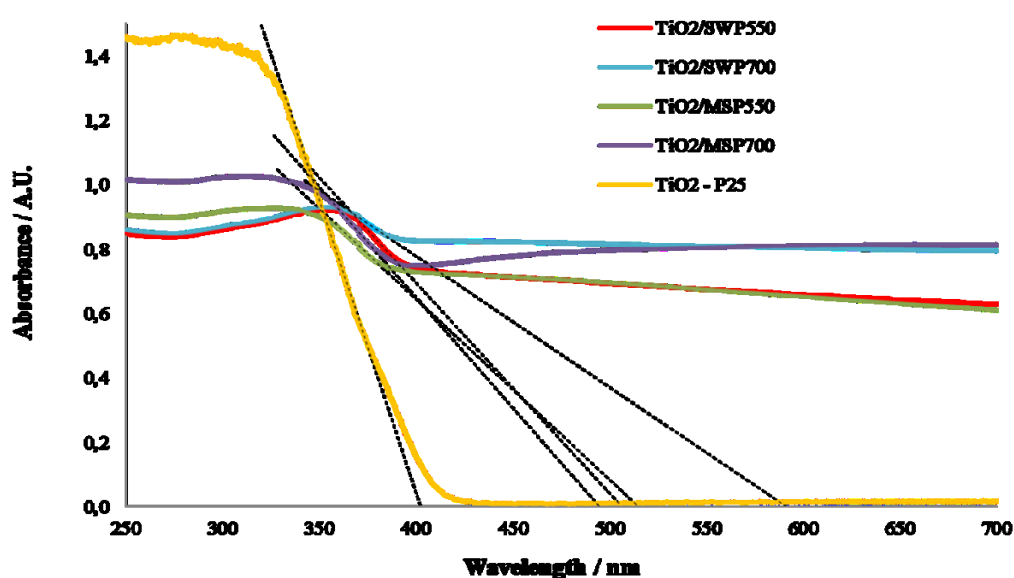


Figure 5. Diffuse reflectance UV-visible spectra of TiO<sub>2</sub>/Biochar materials and TiO<sub>2</sub> P25

The most remarkable differences in band gap energy values among all prepared materials are observed for TiO<sub>2</sub>/SWP700 composite which in turn could be further extended to longer wavelength. Therefore, the improvement in the light absorption and the extended absorption edge may be responsible for the role of SWP700 in the hybrid nanostructures. These observations can suggest an increase of surface electric charge of SWP700, which can lead to modifications of the fundamental process of e<sup>-</sup>/h<sup>+</sup> pair formation while applying visible irradiation. In addition, the introduction of local trap state corresponding to Ti<sup>3+</sup> in TiO<sub>2</sub>/SWP700 (Table 2) can improve the transfer efficiency of electrons between biochar and TiO<sub>2</sub>, which will enhance the photocatalytic redox reactions (Ti<sup>4+</sup> to Ti<sup>3+</sup>). The presence of excess Ti<sup>3+</sup> and oxygen vacancy sites in TiO<sub>2</sub>/SWP700 can cause the visible-light absorption due to the generation of Ti<sup>3+</sup> ions in the bandgap just below the conduction band (CB) of TiO<sub>2</sub>

which lead to a band gap decrease.<sup>21</sup> Furthermore, TiO<sub>2</sub>/SWP700 is considered to take benefit of the SWP700 ability to absorb visible light to initiate the photocatalytic reaction, leading to the formation of some reactive oxidative species.

To investigate the specific role of ultrasound on optical properties, our best performing TiO<sub>2</sub>/SWP700 photocatalyst “in silence” was prepared (Table 1). It is fairly common knowledge that the physical effects of ultrasound can influence the physical and functional properties of materials due to the shear forces generated during acoustic cavitation. It can be stated that TiO<sub>2</sub> (in TiO<sub>2</sub>/SWP700) prepared in “in silence” has higher band gap energy (2.74 eV) than TiO<sub>2</sub> (in TiO<sub>2</sub>/SWP700) prepared by ultrasound-assisted wet impregnation method (2.12 eV). Thus, it can be concluded that ultrasound can act as an “interfacial mediator” in order to improve the visible light photoabsorbability of TiO<sub>2</sub> in TiO<sub>2</sub>/SWP700 composite, while the intimate interfacial contact between SWP700 and TiO<sub>2</sub> may be still retained.

HR XPS surface analysis techniques were performed to evaluate chemistry at the surface of TiO<sub>2</sub>/Biochar materials. The oxidation states and atomic concentrations of Ti 2p, O 1s and C 1s of all TiO<sub>2</sub>/biochar materials as obtained by XPS are given in Table 2. In all prepared materials the dominant bands of Ti 2p are located at binding energies of 461.0±0.2 eV and 459.7 ±0.2 eV and clearly corresponds to Ti<sup>4+</sup> and Ti<sup>3+</sup> in TiO<sub>2</sub> structure.<sup>20-24</sup> In addition, TiO<sub>2</sub>/SWP700 exhibited the highest atomic concentration (0.66 at. %) of Ti<sup>3+</sup> and very high sp<sup>2</sup>/sp<sup>3</sup> ratio (4.0) compared with the other photocatalysts.

Table 2. XPS binding energies and atomic ratio for all prepared composites prepared by ultrasound-assisted wet impregnation method

		Photocatalysts			
		TiO <sub>2</sub> /MSP550	TiO <sub>2</sub> /MSP700	TiO <sub>2</sub> /SWP550	TiO <sub>2</sub> /SWP700
C 1s BE eV (at %)	C-C sp <sup>2</sup>	283.7 (5.19)	283.9 (6.19)	283.8 (32.0)	283.9 (30.11)
	C-C sp <sup>3</sup>	284.8 (2.19)	284.8 (2.82)	284.8 (2.82)	284.9 (7.50)
	C-O-C	286.1 (0.22)	285.9 (1.45)	285.8 (3.47)	286.0 (3.63)
	COOH	287.4 (0.08)	287.6 (0.33)	287.3 (3.47)	287.6 (2.99)
	O=C-O, C=C-OH	-	-	288.5 (2.18)	288.8 (1.96)
	Ti 2p BE eV (at %)	Ti <sup>4+</sup>	460.9 (15.10)	461.1 (14.52)	460.7 (8.49)
	Ti <sup>3+</sup>	459.5 (0.21)	460.0 (0.48)	459.6 (0.57)	459.6 (0.66)
O 1s BE eV (at %)	Ti-O-Ti	529.5 (20.06)	529.8 (26.01)	529.2 (22.63)	529.4 (21.7)

<b>Ti-O</b>	530.6 (26.69)	530,7 (18.71)	530.7 (8.84)	530.3 (12.33)
<b>C-O, C-OH (C-O-C)</b>	532.8 (13.86)	533.0 (14.73)	532.4 (5.39)	532.4 (4.87)

Generally,  $Ti^{3+}$  species in the  $TiO_2$  structure are very important for the heterogeneous photocatalysis due to can trap the photogenerated electrons and leave unpaired charges behind to improve photocatalytic activity.<sup>21</sup> It is also worth pointing out that increasing  $Ti^{3+}$  density promotes effective segregation of electrons, interface charge transfer, and then increases the photocatalytic performance.<sup>21-25</sup> According to the results obtained by the XPS studies, it can be stated that the O/Ti ratios for some samples (especially  $TiO_2$ /SWP700) are slightly below (1.97) the stoichiometric value (O/Ti =2.0). Based on the results obtained, it is expected for this composite the presence of surface oxygen vacancies. These formation of oxygen vacancies on  $TiO_2$ /SWP700 may induce formation of unpaired electrons or  $Ti^{3+}$  centers in order to maintain charge balance. It should be noted that surface  $Ti^{3+}$  defects can interact with  $O_2$  molecules (i.e., a non-dissociative adsorption of  $O_2$  molecule on vacancy defect site), producing the superoxide species,  $O_2^{\bullet-}$ .<sup>23</sup> Interestingly, the presence of surface  $Ti^{3+}$  defects can enhance photocatalytic activity in view of inhibition of the electron-hole recombination<sup>23, 27</sup> and increased oxygen adsorption.<sup>23, 27</sup> This is mainly due to the fact that ultrasound as a “interfacial mediator” can significantly improve the intimate interfacial contact between  $TiO_2$  precursor and SWP700.

The strong bands at  $530.6\text{ eV} \pm 0.2\text{ eV}$  and  $529.5\text{ eV} \pm 0.2\text{ eV}$  are related to the Ti–O and Ti-O-Ti bonds of  $TiO_2$ , which suggests that the chemical state of oxygen is main lattice oxygen in  $TiO_2$ .<sup>28-29</sup> The band at  $532.7\text{ eV} \pm 0.3\text{ eV}$  is corresponding to O–H bond (hydroxyl group), C–O bond and  $H_2O$  adsorbed on the surface of titania.<sup>30-31</sup> The peak of C 1s at around 281-282 eV arising from Ti–C bond was undetectable, strongly suggesting that carbon do not substitute oxygen atom in  $TiO_2$  anatase lattice.<sup>30-31</sup>

Raman spectroscopy was carried out to provides information about  $TiO_2$ /SWP700 and study the  $TiO_2$  form and the carbon matrix (Fig. 6). The spectra showed a representative Raman modes ( $144\text{ cm}^{-1}$  (Eg),  $198\text{ cm}^{-1}$  (Eg),  $394\text{ cm}^{-1}$  ( $B_{1g}$ ),  $514\text{ cm}^{-1}$  ( $B_{1g} + A_{1g}$ ), and  $634\text{ cm}^{-1}$  (Eg)) corresponds to the characteristic peaks of the  $TiO_2$  anatase phase which was also confirmed by HR-TEM (Fig. 7) from which it can be seen that  $TiO_2$  anatase nanoparticle may uniformly carpet the SWP700 surface, suggesting the intimate interfacial contact between

TiO<sub>2</sub> and SWP700. It is worth emphasizing that the peak position (in particular the 144 cm<sup>-1</sup> Eg mode) and the peak width (i.e., full width at half maximum) are in agreement with literature data reported for TiO<sub>2</sub> anatase nanocrystals).<sup>32-33</sup> No peaks either related to rutile or other TiO<sub>2</sub> polymorphs were observed for TiO<sub>2</sub>/SWP700 (confirmed also by XRD). Figure 6 also shows the Raman spectra containing defect-derived D (disorder) peak centered roughly at ~1350 cm<sup>-1</sup> that is related to the presence of sp<sup>3</sup> C–C atoms and G (graphitic) peak at ~1595 cm<sup>-1</sup> that is related to E<sub>2g</sub> phonon of C sp<sup>2</sup> C–C atoms.<sup>34-35</sup>

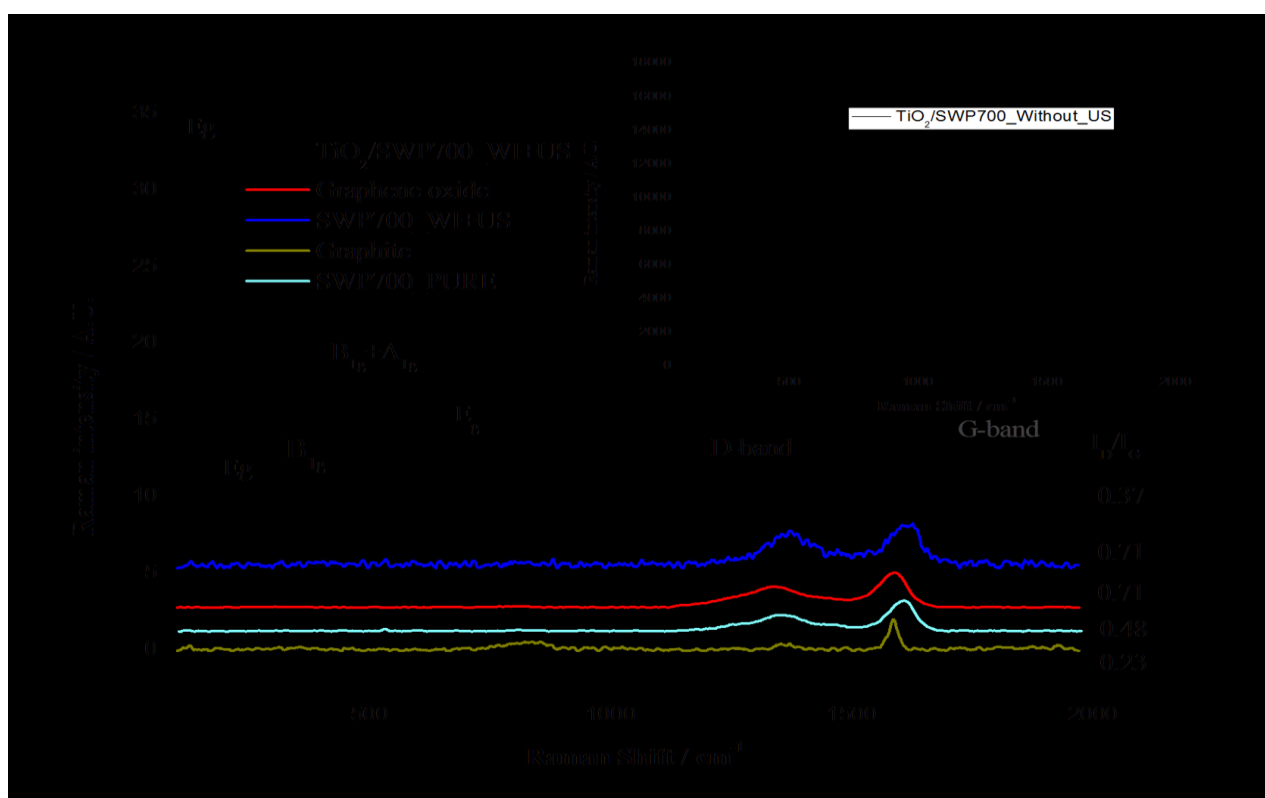


Figure 6. Raman spectra of SWP700 and TiO<sub>2</sub>/SWP700 prepared by ultrasound-assisted wet impregnation method, pure SWP700 carbon materials (graphite and graphene oxide). Inset: TiO<sub>2</sub>/SWP700 prepared without ultrasound.

It is worth noting that the intensity ratio of D-band to G-band ((I<sub>D</sub>/I<sub>G</sub>) ratio), which is important for indication of the amount of functionalization in a carbon material. A high I<sub>D</sub>/I<sub>G</sub> ratio means a high degree of disorder in carbon network.<sup>34-35</sup> If I<sub>D</sub>/I<sub>G</sub> > 1, the structure is more disordered. The intensity ratio of the D-band to G-band (I<sub>D</sub>/I<sub>G</sub>) pointed out disorder in carbon materials such as pure SWP700 (I<sub>D</sub>/I<sub>G</sub>=0.48) and SWP700 treated by ultrasound-assisted wet impregnation method (I<sub>D</sub>/I<sub>G</sub>=0.71) which may be caused by structural surface defects or

disorders within the carbon network, which indicates the difference in micro-structures and SWP700 treated by ultrasound-assisted wet impregnation method had fewer surface defects than pure SWP700. It is worth mentioning that TiO<sub>2</sub>/SWP700 prepared by ultrasound-assisted wet impregnation method showed slightly lower value ( $I_D/I_G=0.37$ ) compared to pure SWP700 ( $I_D/I_G=0.48$ ).

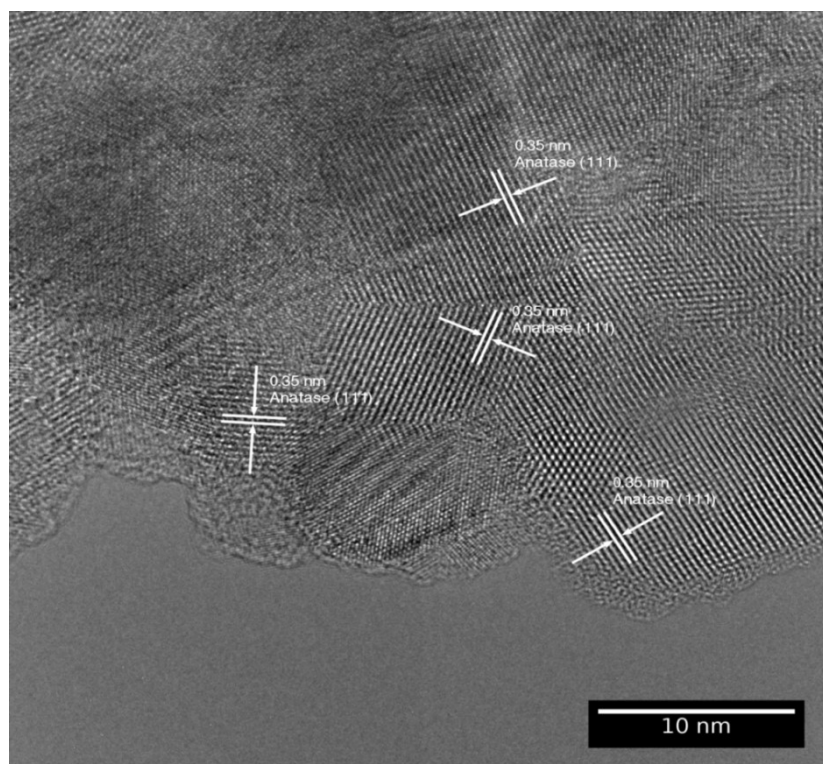


Figure 7. HRTEM micrograph of TiO<sub>2</sub>/SWP700

This decrease might be caused by reconstruction of structural defects within the sp<sup>2</sup> carbon network that arose upon the ultrasound-assisted wet impregnation method and may suggest the existence of conduction network throughout the TiO<sub>2</sub>/SWP700 composite, connecting TiO<sub>2</sub> particles to the conducting SWP700 support. To check the role of ultrasound, TiO<sub>2</sub>/SWP700 without ultrasound was prepared, and in Fig. 6 (inset) the main features of the spectra of this TiO<sub>2</sub>/SWP700 photocatalyst show noticeable variation and without the presence of D and G bands due to a strong fluorescence interference which may suggest high recombination of electrons and holes. It can be stated that, ultrasound can be a “structure-directing factor” for the prepared hybrid material, and the intimate interface connection between SWP700 and TiO<sub>2</sub> can clearly be observed only in the presence of ultrasound as interfacial mediator, indicating that TiO<sub>2</sub> particles were well attached on the SWP700 surface.

## Photocatalytic activity in aqueous phase

All photocatalytic reactions were carried out in a Pyrex cylindrical double-walled immersion well photoreactor. The bath photoreactor was stirred magnetically to obtain a homogenous suspension of the catalyst. A medium pressure 125 W mercury lamp ( $\lambda_{\text{max}} = 365 \text{ nm}$ ), supplied by Photochemical Reactors Ltd. UK (Model RQ 3010) was placed inside the glass immersion well as light irradiation source. The reaction temperature was set at 30 °C. Phenol solution (50 ppm) was prepared in Milli-Q water. Experiments under UV light were performed from 150 mL of the mother solution and 1 g L<sup>-1</sup> of photocatalyst concentration was used after previous optimization. Photocatalytic degradation under visible light were investigated in a glass reactor (V=20 mL) by means of sun-imitating super-quiet Xenon lamp (150 W, L2195 Hamamatsu, 240-2000 nm) with UV/IR-Cut filter (BAADER, blocks UV below 400 nm and IR above 680 nm). The average luminous intensity for UV light (220-400 nm,  $\sim 264.3 \text{ W m}^{-2}$ ) and Visible light (distance between lamp and photoreactor: 8 cm, 400-680 nm,  $\sim 60.6 \text{ W m}^{-2}$ ) was examined by radiometer HD2302.0 (Delta Ohm, Italy). After optimization studies, the optimal adsorption–desorption equilibrium time of 40 min. under dark condition between the photocatalyst and phenol was selected (see Supplementary Information, Fig. S2).

At each sampling point, approx. 1 mL sample was periodically taken from the photoreactor and filtered through 0.2  $\mu\text{m}$ , 25 mm nylon filters to remove photocatalyst. Phenol degradation was measured, after external standard calibration, by a high-performance liquid chromatography (HPLC, Waters Model 590 pump) equipped with a Dual Absorbance Detector (Waters 2487). Separation was performed on an XBridge™ C18 5  $\mu\text{m}$  4.6 x 150 mm column provided by Waters. The mobile phase was Milli-Q water–methanol (65:35 v/v) mixture with 0.1% of CF<sub>3</sub>COOH at a flow rate of 1 mL min<sup>-1</sup>. The injection volume was 10  $\mu\text{L}$ . Blank experiments were performed in the dark as well as with illumination and no catalyst, without observable change in the initial concentration of phenol in both cases.

To investigate the effects of active species generated during the photocatalytic reaction using TiO<sub>2</sub>/SWP700 under UV and Visible illumination, free radicals capture experiments were conducted.<sup>36-37</sup> The three major oxidants involved in photodegradations of organics in water, that is, hydroxyl radical (OH<sup>•</sup>), hole (h<sup>+</sup>), and superoxide radical (O<sub>2</sub><sup>•-</sup>), were trapped by adding 0.5 mL of tert-butanol (t-BuOH), 0.1 mM of ammonium oxalate (AO), and 0.5 mM

of 1,4-benzoquinone (BQ), respectively, into the phenol solutions (see Supplementary Information, Fig. S3).

The photocatalytic activity of all prepared TiO<sub>2</sub>/Biochar composites have been evaluated considering the phenol degradation under UV irradiation (Fig. 8). Negligible phenol degradation (<6%) was noticed in the presence of pure biochar materials during the 4 h illumination and did not find appreciable degradation of phenol in the absence of light (UV and Visible) or photocatalyst. Moreover, the highest phenol degradation was achieved with TiO<sub>2</sub>/SWP700 material (UV light: 64.1%, Visible light: 33.6%) followed by TiO<sub>2</sub>/MSP700 (UV light: 61.3%, Visible light: 27.8%), TiO<sub>2</sub>/NORIT (UV light: 55.1%, Visible light: 29.6%), TiO<sub>2</sub>/SWP550 (UV light: 51.7%, Visible light: 31.2%), and TiO<sub>2</sub>/MSP550 (UV light: 48.1%, Visible light: 26.3%) after 240 min of irradiation. It is worth mentioning that the most active photocatalyst (TiO<sub>2</sub>/SWP700) after 720 minutes of irradiation gave 69.3 % (UV light) and 37.4 % (visible light) phenol degradation in water. The lowest grade of degradation (UV light: 32.8%, Visible light: 9.6%) was achieved with mechanical mixing of 25 wt. % TiO<sub>2</sub> P25/SWP700 photocatalyst. Additionally, TiO<sub>2</sub>/SWP700 photocatalyst prepared “in silence” exhibits low level (UV light: 41.8%, Visible light: 16.5%) of phenol photodegradation, whereas the photocatalyst prepared using ultrasound treatment shows the highest phenol degradation among all photocatalysts after 240 min. of illumination. Furthermore, TiO<sub>2</sub>/SWP700 photocatalyst prepared by ultrasound-based procedures demonstrate higher photocatalytic activity than commercial TiO<sub>2</sub> P25 and SWP700 obtained by mechanically mixing of titania and biochar, which suggests stronger interphase interaction and intimate contact of TiO<sub>2</sub>/SWP700 in the composite photocatalyst than in the physical mixture of TiO<sub>2</sub> P25 and SWP700. In addition, it can be stated that ultrasound may help in increasing the surface active sites of the photocatalysts and also help in binding the TiO<sub>2</sub> on the biochar surface which may enhance the uniform distribution of TiO<sub>2</sub> particles on biochar as clearly seen from SEM images (see Fig. 3). It is worth stressing that during the preparation of TiO<sub>2</sub>-based biochar materials, sonication may play an important role in enhancing the photocatalytic activity of such materials. According to the obtained results, it is observed that TiO<sub>2</sub>/SWP700 showed higher photocatalytic activity and the degradation trend was TiO<sub>2</sub>/SWP700>TiO<sub>2</sub>/MSP700>TiO<sub>2</sub>/NORIT>TiO<sub>2</sub>/SWP550>TiO<sub>2</sub>/MSP550>TiO<sub>2</sub>/SWP700\_ without\_US>TiO<sub>2</sub> P25/SWP700\_mech.mix.

It is worth emphasizing that titanium leaching after the photocatalytic tests was not noticed in the aqueous solution (confirmed by Inductively coupled plasma mass spectrometry (ICP-MS) and XRF, see Supplementary Information: Figure S4) for the best performing

TiO<sub>2</sub>/SWP700 photocatalyst prepared by ultrasound-based procedures. Moreover, it was shown that the photocatalyst TiO<sub>2</sub>/SWP700 prepared without ultrasound suffered from leaching of Ti (0.1 wt.% leaching detected by ICP-MS) in the aqueous solution after 240 min.

All photocatalytic degradation of phenol were performed under natural pH and observed for the best performing material (TiO<sub>2</sub>/SWP700). The pH of the suspension with photocatalyst was checked before irradiation with light (UV and Visible light) and it turned out to be 7.6 and 7.5 respectively. During illumination (3h), the pH value decreased to 6.2 (UV light), 6.3 (Visible light) and again after 4h of illumination it reverted back to 7.1 (UV light) and 7.0 (Visible light). Such processes can be attributed to the formation of organic acidic products obtained in this reaction and a rise in pH after photocatalytic degradation of phenol was owing to mineralization of those organic acidic products.

It is worth mentioning that phenol adsorption capacity in aqueous phase was confirmed by extracting phenol from samples' surface after 240 min of photocatalysis (see Supplementary Information: Table S3). It's worth noting that the highest amount of phenol (~32%) was extracted from the surface of the most active photocatalyst TiO<sub>2</sub>/SWP700 after 240 minutes of reaction which confirms the adsorption capability of this biochar material.

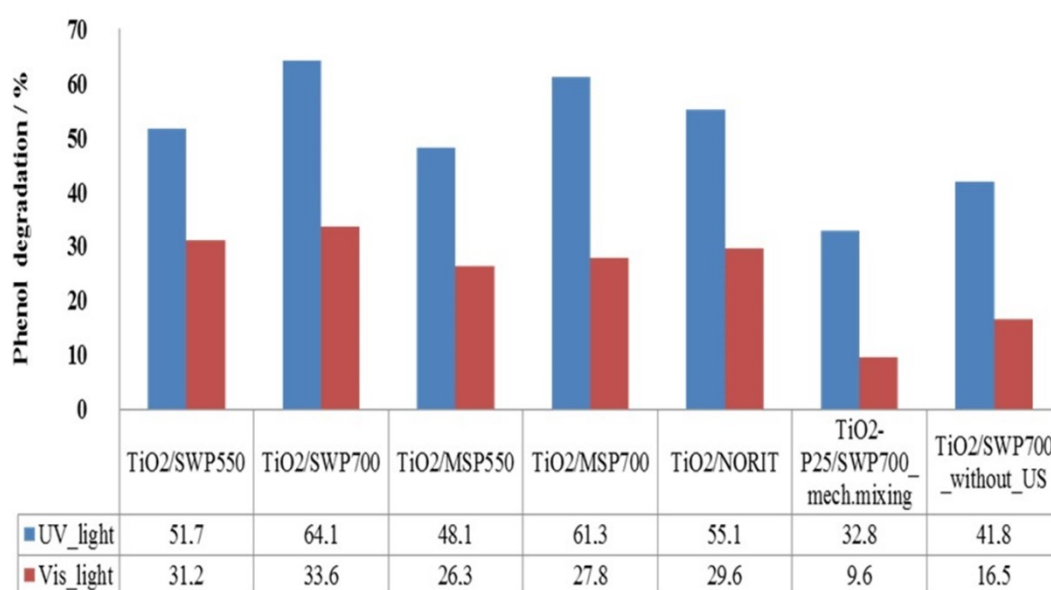


Figure 8. Photocatalytic phenol degradation under UV and visible light over all tested photocatalysts after 240 minutes of illumination.

Chemical Oxygen Demand (COD) is a powerful technique to further verify the degree of mineralization of phenol in aqueous phase. It was observed that TiO<sub>2</sub>/SWP700 showed the highest COD removal with 83.8 % (UV light) and 81.4 % (Visible light), while for SWP700 it was only 12.0 % (UV light) and 12.8 % (Visible light) (see Supplementary Information: Table



S4). These data show that TiO<sub>2</sub>/SWP700 composite photocatalyst does not have considerable difference in COD removals under UV and Visible light (the significant difference is in phenol degradation). It should be noted that when phenol content during the photodegradation of phenol is decreased, more active site and •OH radicals become available to react with phenol and hazardous by-products. In the intermediate phase, by-products were generated from direct oxidation of phenol including aromatic compounds and hydrocarbon chains. All these intermediates can eventually be oxidized to CO<sub>2</sub> via various sub-intermediates following the ring-opening processes.<sup>2, 6-8, 14</sup> On the other hand, another fraction of substrates adsorbed onto SWP700 and without any contact with TiO<sub>2</sub> undergo photodegradation by attack of reactive oxygen species that are generated on the surface of the TiO<sub>2</sub> material but migrate onto the surface of biochar. It is believed that, the ROS (reactive oxygen species) may diffuse over sub-millimeter distances from the surface of TiO<sub>2</sub>, so some ROS can reach the target compound situated on the surface of the biochar, where most of the phenol remains adsorbed.

The reuse of any photocatalyst is very important for its water treatment application. In order to assess the long-term performance of the composite photocatalyst, a recycling test for phenol degradation was carried out. After each cycle, the photocatalyst was filtered out and left to dry at 110 °C overnight before use in the next cycle. To evaluate the stability and reusability of our best photocatalytic material (TiO<sub>2</sub>/SWP700), successive cycles of the photocatalytic phenol degradation were carried out (Fig. 9) under the same reaction conditions with the loss of only ~ 10 % of phenol degradation activity after run 5. The results revealed that the photocatalytic activity of TiO<sub>2</sub>/SWP700 photocatalyst has promising cyclic stability.

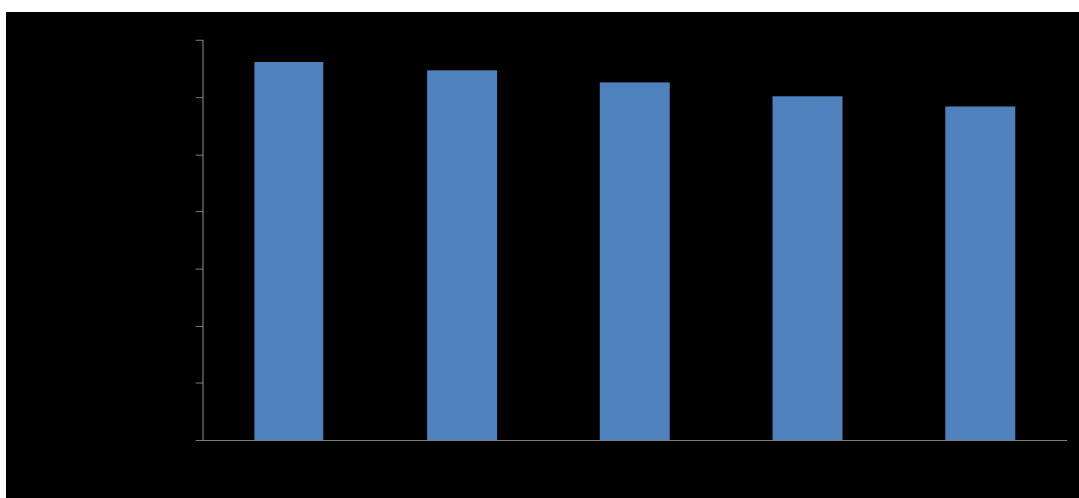
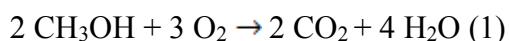


Figure 9. Multi-cycle performance of TiO<sub>2</sub>/SWP700 photocatalyst in photocatalytic phenol degradation

## Photocatalytic activity in gas phase

The schematic view of the photocatalytic reaction system in the gas phase is shown in Figure 10. After achieving reagent–photocatalyst adsorption equilibrium in the dark (after 2 h), liquid methanol was fed into the photocatalytic reaction system by a programmable syringe pump (NE-1000, Syringe Pump Com.) at a constant flow rate of  $1.5 \mu\text{L min}^{-1}$ . The whole reactor system lines were heated to prevent condensation. This gas mixture containing 0.9 vol. % of methanol and 99.1 vol. % of air was supplied at a flow rate of  $25 \text{ cm}^3\text{min}^{-1}$  into the photoreactor. The gas flow rates were measured and controlled by mass flow controllers (Bronkhorst HI-TEC). The continuous fixed-bed photoreactor was vertically enclosed by an aluminum foil cylindrical reflector (20 cm x 13 cm x 1 mm) to exclude any external light source and maximize light energy usage within the reactor. The light source was a medium pressure 125 W mercury lamp ( $\lambda_{\text{max}} = 365 \text{ nm}$ ), supplied by Photochemical Reactors Ltd. UK (Model RQ 3010) and sun-imitating Xenon lamp (150 W, L2195 Hamamatsu, 240-2000 nm) with UV/IR-Cut filter (BAADER, blocks UV below 400 nm and IR above 680 nm) built into a lamp housing and centered vertically in the reflector (2.5 cm between the lamp and photoreactor) and thermostated at  $30 \text{ }^\circ\text{C}$ . The average luminous intensity for UV light (220-400 nm,  $\sim 274.9 \text{ W m}^{-2}$ ) and Visible light (400-680 nm,  $\sim 271.5 \text{ W m}^{-2}$ ) was examined by radiometer HD2302.0 (Delta Ohm, Italy). Reaction products were quantitatively analyzed by means of online gas chromatography (HP 5890 series II Hewlett Packard USA equipped with a flame ionization detector (FID) and a methanizer model 510 instrument supplied by SRI INSTRUMENTS) and identified offline by GC–MS (HP-5 column GC (6890 Series)–MS(5973) Hewlett Packard equipped with FID).

To understand better the impact of gas phase reactions on all synthesized materials, selective photooxidation of methanol were performed. After 240 minutes of illumination,  $\text{CO}_2$  and methyl formate (MF) were detected as the only two reaction products by using the following equations (1) and (2):



Photocatalyst efficiency was calculated according to methanol conversion (X), yield (Y), and selectivity (S) of methyl formate on the basis of equations (3), (4) and (5):<sup>38</sup>

Conversion (X) of CH<sub>3</sub>OH:

$$X (\%) = \frac{(\text{Moles of } CH_3OH^{in} - \text{Moles of } CH_3OH^{out})}{\text{Moles of } CH_3OH^{in}} \times 100 \quad (3)$$

Yield (Y) of HCOOCH<sub>3</sub>:

$$Y (\%) = \frac{2 \times \text{Moles of } HCOOCH_3^{products}}{\text{Moles of } CH_3OH^{in}} \times 100 \quad (4)$$

Selectivity (S) of HCOOCH<sub>3</sub>:

$$S (\%) = \frac{\text{Moles of } HCOOCH_3^{products}}{\text{Moles of } (HCOOCH_3 + CO_2)} \times 100 \quad (5)$$

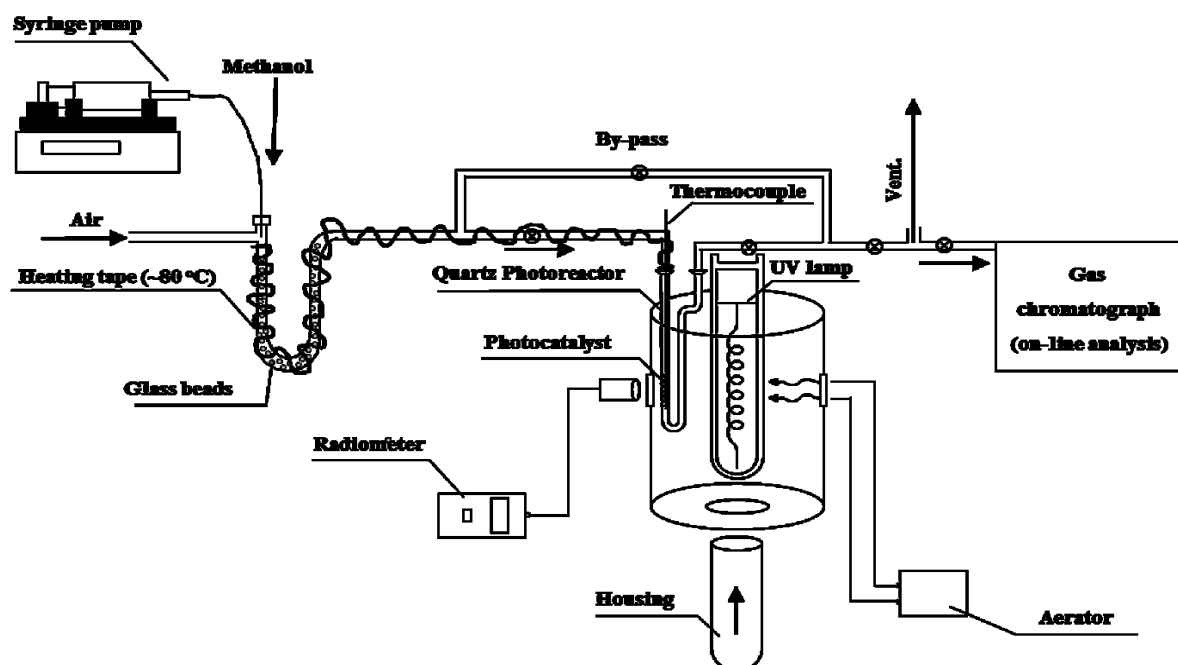


Figure 10. Schematic view of the photocatalytic reaction system in the gas phase

Starting with the control tests in the gas phase, two tests were done: (1) photocatalytic reaction in gas phase (UV lamp and air flow) without photocatalyst and (2) photocatalytic reaction in gas phase (No UV light, air flow and at the temperature up to 100 °C) in the presence of photocatalyst (the results of these experiments are not presented here). Photolysis (without photocatalyst) revealed negligible conversion of methanol (~5%). Thermal test up to 100 °C, TiO<sub>2</sub>/SWP700 photocatalyst was not active. It should be also noted that, GC on-line analysis did not show any leaching of carbon (SWP700) during the photocatalytic test in gas phase for the best performing TiO<sub>2</sub>/SWP700 photocatalysts (stability test: air flow (25 cm<sup>3</sup>min<sup>-1</sup>), UV illumination and absence of methanol). Figure 11 shows the results photo-

oxidation of methanol over all TiO<sub>2</sub>/Biochar together with that of the TiO<sub>2</sub>/NORIT photocatalyst for comparison. Additionally, none of the pure biochar were active in the photo-oxidation of methanol. It is worth emphasizing that the TiO<sub>2</sub>/SWP700 photocatalyst achieved the highest conversion of methanol (~90%) of all tested composites, high methyl formate production (~80 %) and high yield of methyl formate (~88 %) after 240 minutes of illumination. After changing the light source to visible range, all hybrid materials exhibited lower methanol conversion (< 7%) after 240 minutes of illumination.

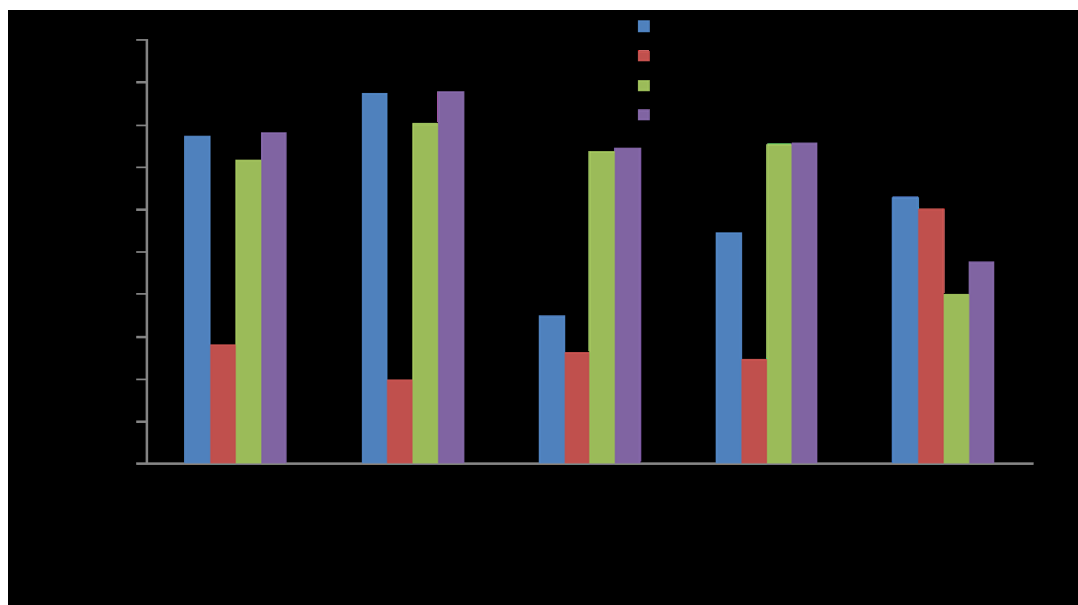


Figure 11. Photo-oxidation of methanol in gas phase over all tested photocatalysts after 240 minutes of illumination.

It should be also noted that, TiO<sub>2</sub>/SWP700 prepared without ultrasound (results not shown) gave 65.3 % methanol conversion, and selectivity to MF of 67.1 % and to CO<sub>2</sub> of 30.6 % after 240 minutes of illumination. Meanwhile, photo-oxidation of methanol without oxygen (argon instead of air), the TiO<sub>2</sub>/SWP700 photocatalyst exhibited extremely low methanol conversion (~ 4%). According to the obtained results, it is observed that TiO<sub>2</sub>/SWP700 exhibits the highest photocatalytic activity/selectivity in terms of methanol/MF conversion/selectivity, and the trend is TiO<sub>2</sub>/SWP700 >TiO<sub>2</sub>/SWP550 >TiO<sub>2</sub>/NORIT >TiO<sub>2</sub>/MSP700 > TiO<sub>2</sub>/MSP550.

The study of the reusability and sequential application of synthesized photocatalysts is an important factor for future applications, and therefore with this in mind, the cyclic performance of TiO<sub>2</sub>/SWP700 was investigated in five consecutive runs of photo-oxidation of methanol. The results of the catalytic long-run stability tests are shown in Fig. 12. During this

experiment, after each run of 240 minutes of illumination, the TiO<sub>2</sub>/SWP700 photocatalyst was "cleaned" in a 25 mL min<sup>-1</sup> flow of air at room temperature to remove all physisorbed reagents and products from the photocatalyst surface (monitoring by GC online analysis), and then the photocatalyst was used for the following run (lamp "on"). It should be emphasized that, our best photocatalytic material (TiO<sub>2</sub>/SWP700) successive cycles of the photo-oxidation of methanol under the same reaction conditions with the loss of only ~ 10 % of photocatalytic conversion after run 5 (20 h of illumination).

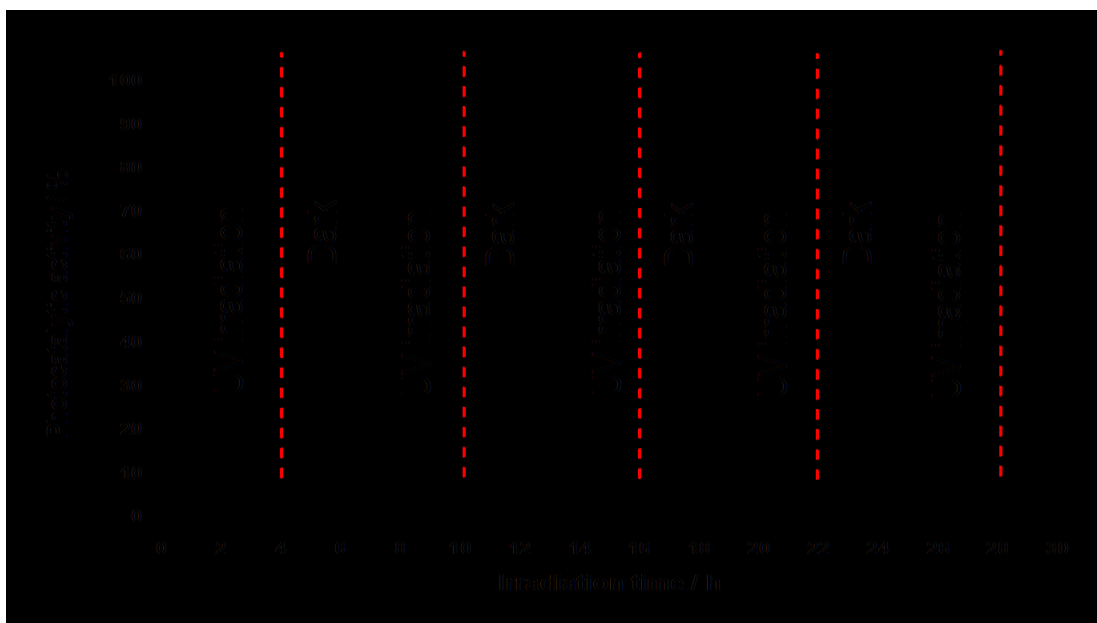


Figure 12. Photocatalytic activity of TiO<sub>2</sub>/SWP700 in long-run test of photocatalytic oxidation of methanol in gas phase

### **Tentative oxidative transformations pathways of the best performing photocatalyst (TiO<sub>2</sub>/SWP700) in aqueous and gas phase**

FT-IR is very informative in the determination of various functional groups on TiO<sub>2</sub>/SWP700 (Fig. 13) materials before and after photocatalytic phenol degradation (liquid phase) and selective oxidation of methanol (gas phase). While FTIR spectrum of pure SWP700 in this region were not clearly resolved (no functional groups), the spectra of TiO<sub>2</sub>/SWP700 after illumination in gas and liquid phase showed additional peaks. The broad peak in the 3200-3600 cm<sup>-1</sup> region suggests that the TiO<sub>2</sub>/SWP700 surface is rich in hydroxyl groups, which can be an evidence for the existence of Ti-OH.<sup>30, 39-41</sup> For this reason, H<sub>2</sub>O are easily adsorbed on the surface of this high BET of biochar based photocatalyst. The main peaks appearing in the range 2900-3000 cm<sup>-1</sup> correspond to methoxy species (vs(CH<sub>3</sub>)) and

$2\delta_2(\text{CH}_3)$  of  $\text{CH}_3$  in adsorbed  $\text{OCH}_3$ ).<sup>42-48</sup> Bands observed in the  $1730\text{--}1780\text{ cm}^{-1}$  and  $1600\text{--}1650\text{ cm}^{-1}$  regions correspond to  $\text{C}=\text{O}$  vibrations of  $\text{COOH}$ ,  $\text{O}=\text{C}-\text{O}$  and  $\text{C}=\text{C}-\text{OH}$ .<sup>39-40, 43, 45, 46-48</sup> The bands in the range  $450\text{--}550\text{ cm}^{-1}$  were assigned to  $\text{Ti}-\text{O}$  vibration.<sup>41, 49-50</sup> In addition, the FT-IR bands in  $700\text{--}900\text{ cm}^{-1}$  pointed out  $\text{Ti}-\text{O}-\text{Ti}$  bond in the  $\text{TiO}_2$  anatase phase.<sup>41, 43-50</sup> After UV illumination of  $\text{TiO}_2/\text{SWP700}$  in liquid phase (Fig. 13,  $\text{TiO}_2/\text{SWP700\_AR\_liquid phase}$ ), peaks appearing in the range  $2400\text{--}2500\text{ cm}^{-1}$  and  $750\text{--}900\text{ cm}^{-1}$  correspond to gaseous  $\text{CO}_2$ <sup>40, 46-53</sup> and the above-mentioned  $\text{Ti}-\text{O}-\text{Ti}$  band, respectively. In the case of  $\text{TiO}_2/\text{SWP700}$  after UV illumination in gas phase (Fig. 13,  $\text{TiO}_2/\text{SWP700\_AR\_gas phase\_MeOH}$ ), new bands appeared and correspond to gaseous  $\text{CO}_2$  associated with total oxidation of methanol ( $2400\text{--}2500\text{ cm}^{-1}$ ) and  $\text{C}-\text{O}$  band from methanol ( $1020\text{--}1070\text{ cm}^{-1}$ )<sup>42, 46-47</sup> which appear during photocatalytic oxidation of methanol in gas phase. Moreover, new bands at  $1360$ ,  $1380$  ( $\nu_s(\text{OCO})$ ), and  $1580\text{ cm}^{-1}$  ( $\nu_{as}(\text{OCO})$ ) may correspond to adsorbed formate species.<sup>46-48, 54</sup>

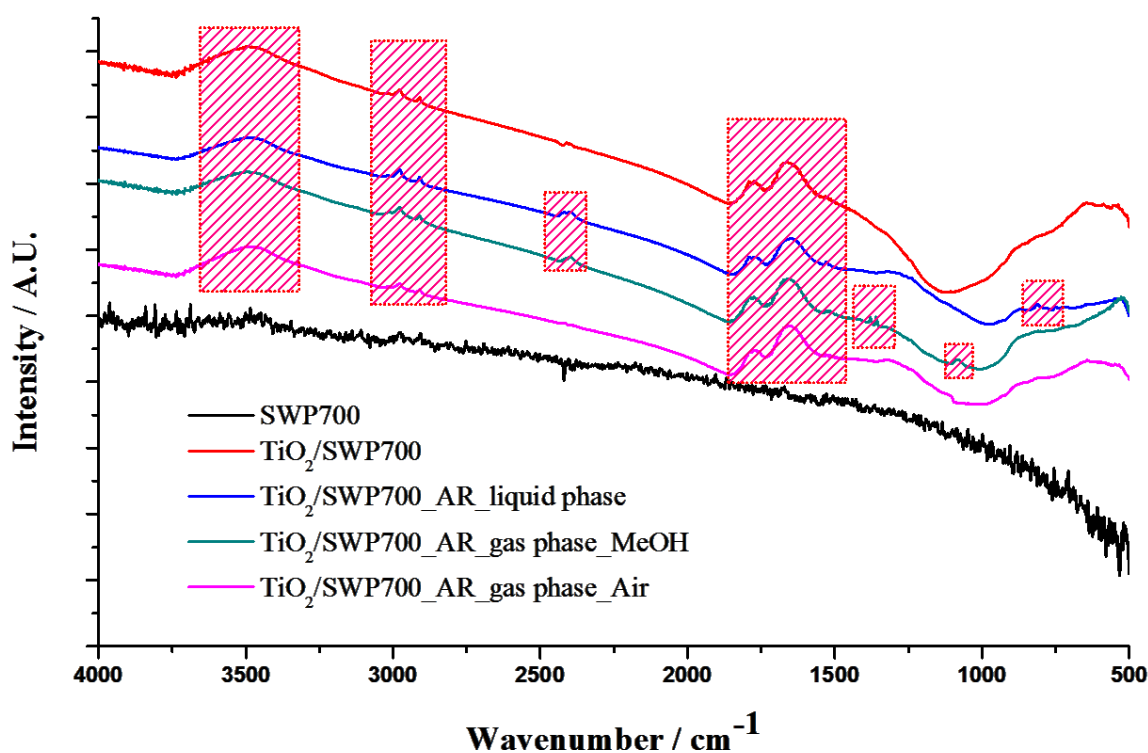


Figure 13. FTIR spectra for SWP700 and  $\text{TiO}_2/\text{SWP700}$  photocatalyst. The suffix “AR” stands for “after reaction”.

The HR XPS spectrum (Table S5: Supplementary Information) of  $\text{C } 1s$  indicates that the surface of SWP700 and  $\text{TiO}_2/\text{SWP700}$  treated by “ultrasound-assisted wet impregnation

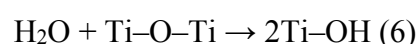
method” have strong bands at  $287.3 \pm 0.3$  eV and  $288.6 \pm 0.2$  eV clearly corresponds to COOH, O=C-O and C=C-OH in comparison with pure SWP700 and TiO<sub>2</sub>/SWP700 (without ultrasound) which don't have O=C-O and C=C-OH surface functional groups and weaker bands corresponds to COOH in the case of TiO<sub>2</sub>/SWP700 (without ultrasound). These results confirm that the presence of surface functional groups favored the deposition of TiO<sub>2</sub> on biochar (SWP700) surface and reveal a better interaction between TiO<sub>2</sub> precursor and SWP700. The presence of these functional groups might be necessary to improve the dispersion of TiO<sub>2</sub> where the carboxylic groups can play significant role as anchoring groups for titanium tetraisopropoxide (TiO<sub>2</sub> precursor). Based on the experimental evidence presented in the table S5 (see SI), we can state that there was a significant increase in C-C sp<sup>2</sup> atoms in the presence of TiO<sub>2</sub>/SWP700 after photocatalytic reaction in liquid (16.31 at %) and gas phase (2.18 at %) with remarkable decrease of TiO<sub>2</sub>/SWP700 prepared “in silence” (20.5 at %). Such results show the important effect of sonication as a “interfacial mediator” on the C-C sp<sup>2</sup> surface functional groups which can significantly improve the intimate interfacial contact between SWP700 and TiO<sub>2</sub>. It is well known that, C-C sp<sup>2</sup> surface functional groups can act as scattering centres which may provide exceptional electrical and optical properties, high resistivity and electron mobility in carbon materials.<sup>55-58</sup>

The measured photoluminescence (PL) emission spectra of SWP700 and TiO<sub>2</sub>/SWP700 prepared by ultrasound-based procedures and TiO<sub>2</sub>/SWP700 prepared without ultrasound are presented in Fig. S5 (Supplementary information). It is well known that the lower photoluminescence emission spectra points out the lower recombination rate of photogenerated e<sup>-</sup>-h<sup>+</sup> pairs, which leads to the high photocatalytic activity of semiconductor photocatalysts.<sup>59-61</sup> Consequently, the very low photoluminescence emission spectra for TiO<sub>2</sub>/SWP700 prepared by ultrasound-assisted wet impregnation method points out that the photocatalytic efficiency of TiO<sub>2</sub> may be improved owing to the intimate contact of the TiO<sub>2</sub> and SWP700 through a heterostructure vicinity. As a result of excitation irradiation, biochar as an electron collector and transporter can benefit the charge transfer in the TiO<sub>2</sub>/SWP700 and inhibit the charge recombination. It is generally accepted that the PL spectrum with low intensity indicates efficiently separation of the charge carriers, leading to participation of more electrons and holes in the oxidation and reduction reactions. However, there is a considerable decrease in the intensity of the PL spectrum for TiO<sub>2</sub>/SWP700 prepared by ultrasound-assisted wet impregnation method compared to that of TiO<sub>2</sub>/SWP700 prepared “in silence”. These observations suggest the formation of a heterojunction formed at the interface

between TiO<sub>2</sub> and SWP700 in the presence of ultrasound, which confirms an excellent electron-hole separation efficiency of the composite material, hence enhanced photocatalytic performance can be acquired in this study.

### **Tentative degradation pathway of photocatalytic reaction in aqueous phase**

Based on the experimental evidence presented, and under our reaction conditions, we can state that our best photocatalyst (TiO<sub>2</sub>/SWP700) achieved 64.1% (UV light) and 33.6% (Visible light) of phenol degradation. In order to gain further insight into photocatalytic mechanism, trapping experiment of active species were performed to observe the active species generated during the photocatalytic process. It's observed that h<sup>+</sup>, <sup>•</sup>OH and <sup>•</sup>O<sub>2</sub><sup>-</sup> may be involved in photocatalytic degradation of phenol under UV and Visible illumination (SI, Fig. S3). In addition, TiO<sub>2</sub>/SWP700 photocatalyst can efficiently transfer photo-induced electrons to reduce the recombination of e<sup>-</sup>-h<sup>+</sup> pairs which are trapped or react in aqueous phase producing reactive species such as <sup>•</sup>OH and <sup>•</sup>O<sub>2</sub><sup>-</sup>. <sup>•</sup>OH radicals were formed on the surface of TiO<sub>2</sub>/SWP700 by the reaction of holes with adsorbed water and/or surface functional groups like Ti-OH and Ti-O-Ti (based on FTIR (Fig. 13) and XPS which showed lower at. % of Ti-O-Ti after reaction (SI, Table S5)), which may be attributed to enhance efficiency in photodegradation of phenol. Additionally, hydroxyl groups on the surface of TiO<sub>2</sub>/SWP700 can be responsible for the reaction of adsorbed water with titania and creation of Ti-OH according to the following reaction (6):



TiO<sub>2</sub>/SWP700 with the highest surface Ti<sup>3+</sup> species (0.66 at %), compare to other photocatalysts, can reduce the recombination between trapped electrons Ti<sup>3+</sup> and trapped holes (Ti-OH and Ti-O-Ti) and thanks to interfacial interaction of SWP700 and TiO<sub>2</sub>, more electrons and holes were transferred. Additionally, the excellent support of SWP700 which can act as electron mediator to the photogenerated electrons of TiO<sub>2</sub> from the conduction band (CB) with a quick transfer to the surface of SWP700 and then reaction with O<sub>2</sub> absorbed on its surface or dissolved in water to produce <sup>•</sup>O<sub>2</sub><sup>-</sup> by photogenerated electrons. Meanwhile, OH<sup>-</sup> or H<sub>2</sub>O can be oxidized to hydroxyl radicals (<sup>•</sup>OH) by the photogenerated holes, and the <sup>•</sup>OH radicals and/or Ti-OH and Ti-O-Ti can directly attack the phenyl ring of phenol yielding degradation products including aromatic compounds and hydrocarbon chains and subsequently these intermediates were completely mineralized to carbon dioxide and water.<sup>13-</sup>



<sup>14 62-64</sup>. Therefore,  $h^+$ ,  $\cdot OH$  and  $\cdot O_2^-$  (all of them observed in the photocatalytic activity) function as ROS in the photocatalytic reactions.

To further understand the potential role of molecular oxygen in the complex photocatalytic mechanism, photocatalytic reactions of phenol in the absence of oxygen (argon instead of air) were carried out. It should be noted that, our best performing photocatalyst  $TiO_2/SWP700$  photocatalyst in the absence of oxygen resulted in phenol degradation of 36.1 % (UV light) and 18.4 % (visible light). It is necessary to emphasize that the reaction of molecular oxygen with photogenerated electrons for the generation of  $\cdot O_2^-$  is important for photodegradation of phenol over  $TiO_2/SWP700$ . From this point of view, relatively high surface area ( $399\text{ m}^2\text{g}^{-1}$ ), 100% anatase phase and strong adsorption ability for phenol, the relative narrower band-gap of  $TiO_2/SWP700$  composites (2.12 eV) and more harvesting of visible light owing to the presence of SWP700, lower recombination rate of the photoexcited  $e^-h^+$  pairs prolong the lifetime of a photogenerated carrier, thus greatly improving the photocatalytic efficiency and stability of  $TiO_2/SWP700$  composites in the removal of phenol. Finally, it should be noted that the presence of higher percentage of C-C  $sp^2$  surface functional groups (confirmed by HR-XPS) on the  $TiO_2/SWP700$  may be also attributed to enhance efficiency in the photocatalytic reaction in aqueous phase.

### **Tentative oxidation pathway of photocatalytic selective reaction in gas phase**

To get some insights into the plausible reaction pathway of photocatalytic reaction in gas phase, a set of FT-IR measurements of  $TiO_2/SWP700$  were carried out (Fig. 13). During light irradiation, methanol is converted to a greater extent, and FT-IR band intensity associated with adsorbed intermediate methoxy species, hydroxyl species, formate species and gaseous  $CO_2$ . The presence of adsorbed formate molecules during the oxidation of methanol to methyl formate is not uncommon, and these have been suggested to formation upon the reaction of surface oxygen with adsorbed formaldehyde.<sup>54, 65-66</sup> It should be also noted that, photocatalytic methanol photooxidation would be expected if significant UV radiation was incident on the  $TiO_2/SWP700$  photocatalysts and, as consequence, the surface hydroxyl groups on prepared composite might also can play a vital role in the photocatalytic reaction, as these groups can inhibit the recombination of photogeneration charges.<sup>1, 3, 22-25</sup> It's well known that methyl formate is formed by the reaction of adsorbed formaldehyde and adsorbed methoxy species, which is reported to take place when the two are in close proximity on the photocatalyst surface.<sup>67-68</sup> Nevertheless, formate molecules on the catalyst

surface can react with methanol<sup>69</sup> to form methyl formate as an alternative route, suggesting the importance of formate species during the reaction. The presence of formate species on the surface (which are available to react with methanol) are confirmed on the photocatalyst surface during the photo-oxidation of methanol in the frame of the present research work. Surface adsorbates, particularly formate species, build up on the photocatalyst surface of TiO<sub>2</sub>/SWP700 during the photooxidation reaction and enhanced the photo-oxidation of methanol. On the other hand, O<sub>2</sub> adsorbed on the surface of TiO<sub>2</sub>/SWP700 may accept the electron and form the <sup>•</sup>OH radical<sup>70-71</sup> which oxidizes the adsorbed molecules directly on the surface. The same mechanism could explain the enhanced photocatalytic efficiency of TiO<sub>2</sub>/SWP700 composites tested for the photocatalytic oxidation of methanol in gas phase. Mo and Ye<sup>71</sup> reported that various oxygen species like crystal lattice oxygen (O<sub>2</sub><sup>-</sup>) (~528.8 eV), hydroxyl oxygen (O<sup>-</sup>) (~530.6 eV), and adsorbed oxygen (O<sub>2</sub><sup>-</sup>) (~532.1 eV) may appear, which was confirmed by XPS analysis in our case. Based on experimental evidence presented in Table S5 (see SI), we can state that there was a significant increase in oxygen surface species such as crystal lattice oxygen (O<sub>2</sub><sup>-</sup>) (0.31 at %), the hydroxyl oxygen (O<sup>-</sup>) (0.84 at %), and the adsorbed oxygen (O<sub>2</sub><sup>-</sup>) (3.52 at %) in the presence of TiO<sub>2</sub>/SWP700 after the photocatalytic oxidation in gas phase. Not only adsorbed oxygen species (O<sub>2</sub><sup>-</sup>) but also surface hydroxyl oxygen species (O<sup>-</sup>) were very favourable for the photocatalytic oxidation reaction.<sup>26, 72-73</sup> Nevertheless, the hydroxyl oxygen species (O<sup>-</sup>) could produce active species (<sup>•</sup>OH free radical). Consequently, the adsorbed oxygen species (O<sub>2</sub><sup>-</sup>) on the surface and their adsorption and diffusion properties can be dominant for transportation process of various oxygen species in the photocatalytic oxidation<sup>26, 74</sup> and could be responsible for photocatalytic oxidation of methanol to methyl formate in the presence of TiO<sub>2</sub>/SWP700. Interesting is the fact that the peroxy radicals (<sup>•</sup>O<sub>2</sub>) generated after this electron capture could accelerate the oxidation of organic substances and the adsorbed oxygen species (O<sub>2</sub><sup>-</sup>) can serve as the capturer or taker of photogenerated electrons.<sup>73-74</sup> Additionally, the adsorbed O<sub>2</sub> also served as an oxidant, which can control the recombination of photo induced electron-hole recombination.<sup>74</sup> Consistently, the observed increase in adsorbed oxygen species on the photocatalyst surface could be responsible for the enhanced activity in the selective oxidative esterification of methanol to methyl formate in continuous gas phase (high activity (~90%), high selectivity to methyl formate (~80 %) and high yield of methyl formate (~88 %)) after 240 minutes of illumination under UV light. The results may confirm that coupling of TiO<sub>2</sub> with SWP700 by a good interfacial contact significantly facilitates the charge carrier transfer process upon ultraviolet illumination. Concurrently, this is the first direct and robust experimental evidence to show

the role of SWP700 which can behave as an electron reservoir to capture or shuttle photogenerated electrons from the semiconductor upon light irradiation in selective photo-oxidation of methanol in gas phase.

## **Conclusions**

This paper was aimed to illustrate a low-cost, efficient and environmentally friendly approach to synthesize and significantly improve the photoactivity of titania-based wood (Soft Wood Pellets (SWP)) and straw-derived (Miscanthus Straw Pellets (MSP)) composites. This was achieved by using ultrasound assisted methodology that promoted formation of intimate interfacial contact between biochar and TiO<sub>2</sub>. Such interfacial composition chemistry not only optimizes the photogenerated charge carrier transfer pathway across the interface between biochar and TiO<sub>2</sub> but also efficiently improves the lifetime/transfer of charge carriers (low recombination rate) in the heterostructure TiO<sub>2</sub>/Biochar systems (especially TiO<sub>2</sub>/SWP700) but also significantly influences the physicochemical properties of prepared hybrid materials. The best performing TiO<sub>2</sub>/SWP700 photocatalyst exhibited favorable properties, such as 100% anatase nanoparticles, visible light absorption and high surface area, and enhanced photocatalytic activity/selectivity in liquid and gas phase. Importantly, TiO<sub>2</sub>/SWP700 was the most photocatalytically active (without Ti leaching) in phenol photodegradation (UV light: 64.1 %, Visible light: 33.6 %) and photocatalytic selective reaction with extraordinarily high activity (~90%), high selectivity to methyl formate (~80 %) and high yield of methyl formate (~88 %) after 240 minutes of illumination. Obtained results revealed the existence of an intimate contact between SWP700 and TiO<sub>2</sub> phases in the composite photocatalysts capable of attaining unique electron transfer properties on the resulting composites. Thus it can be concluded that ultrasound can act as a “interfacial mediator” and may lead to improved visible light photoabsorbability of TiO<sub>2</sub>/SWP700 composite and promotes the creation of an intimate heterojunction formed at the interface between TiO<sub>2</sub> and SWP700 in the presence of ultrasound and by this explaining the excellent electron-hole separation efficiency of the composite material. This work offers a simple, economic and powerful tool to prepare TiO<sub>2</sub>/biochar photocatalysts with high photocatalytic activity and stability. This is an important step ahead in development of viable applications of photocatalysts in water treatment sector and new approaches for organic synthesis. This work makes an important contribution to the application of renewable, biomass-based materials as well as their utilization in effective photocatalytic processes for environmental management.

## Supporting Information

Detailed experimental procedures for materials characterization and measurements; Nitrogen adsorption–desorption isotherms over all tested photocatalysts; Table with characteristics of four standard biochar's; Table with the BET surface area of biochar and TiO<sub>2</sub>/Biochar materials; Phenol adsorption equilibrium curves over all tested photocatalysts in the dark; Evaluation of the effect of different scavengers on the photodegradation of phenol in aqueous phase; XRF analysis of the aqueous solution; Table with results of extracting phenol from samples' surface; COD removal; Photoluminescence spectra; Table with HR XPS.

**Acknowledgements:** This work was supported by the National Science Centre (NCN) in Poland within research project 2015/17/N/ST5/03330. We would also like to thank the COST Association (Action FP1306) for supporting the dissemination of this work. The authors thank Dr. K. Sobczak, Institute of Physics, PAS in Poland for HRTEM images.

## Reference

- (1) Pelaez, M.; Nolan, N.T.; Pillai, S.C.; Seery, M.K.; Falaras, P.; Kontos, A.G.; Dunlop, P.S. M.; Hamilton, J.W.J.; Byrne, J.A.; O'Shea, K.; Entezari, M.H.; Dionysiou, D.D. A review on the visible light active titanium dioxide photocatalysts for environmental applications. *Appl. Catal., B* **2012**, *125*, 331-349, DOI: <https://doi.org/10.1016/j.apcatb.2012.05.036>.
- (2) Liu G.; Wang, L.; Yang, H.G.; Cheng, H.M.; Lu, G.Q. Titania-based photocatalysts-crystal growth, doping and heterostructuring. *J. Mater. Chem.* **2010**, *20*, 831-843, DOI: 10.1039/B909930A.
- (3) Ng, Y.H.; Ikeda, S.; Matsumura, M.; Amal, A. A perspective on fabricating carbon-based nanomaterials by photocatalysis and their applications. *Energy Environ. Sci.* **2012**, *5*, 9307-9318, DOI: 10.1039/C2EE22128D.
- (4) Qu, Y.; Duan, X. Progress, challenge and perspective of heterogeneous photocatalysts. *Chem. Soc. Rev.* **2013**, *42*, 2568-2580, DOI: 10.1039/C2CS35355E.
- (5) Su, D.S.; Perathoner, S.; Centi, G. Nanocarbons for the development of advanced catalysts. *Chem. Rev.* **2013**, *113*, 5782-5816, DOI: 10.1021/cr300367d.
- (6) Leary, R.; Westwood, A. Carbonaceous nanomaterials for the enhancement of TiO<sub>2</sub> photocatalysis. *Carbon* **2011**, *49*, 741-772, DOI: <https://doi.org/10.1016/j.carbon.2010.10.010>.
- (7) Colmenares, J.C.; Varma, R.S.; Lisowski, P. Sustainable hybrid photocatalysts: titania

immobilized on carbon materials derived from renewable and biodegradable resources. *Green Chem.* **2016**, *18*, 5736-5750, DOI: 10.1039/C6GC02477G.

(8) Liu, W.J.; Jiang, H.; Yu, H.Q. Development of biochar-based functional materials: toward a sustainable platform carbon material. *Chem. Rev.* **2015**, *115*, 12251-12285, DOI: 10.1021/acs.chemrev.5b00195.

(9) Kim, J.R.; Kan, E. Heterogeneous photocatalytic degradation of sulfamethoxazole in water using a biochar-supported TiO<sub>2</sub> photocatalyst. *J. Environ. Manage.* **2016**, *180*, 94-101, DOI: <https://doi.org/10.1016/j.jenvman.2016.05.016>.

(10) Matos, J. Eco-friendly heterogeneous photocatalysis on biochar-based materials under solar irradiation. *Top. Catal.* **2016**, *59*, 394-402, DOI: 10.1007/s11244-015-0434-5.

(11) U.S. Environmental Protection Agency. *The Inside Story: A Guide to Air Quality; Office of Radiation and Indoor Air (6609J)*, Washington, DC, USA, **2009**.

(12) Mo, J.; Zhang, Y.; Xu, Q.; Lamson, J.J.; Zhao, R. Photocatalytic purification of volatile organic compounds in indoor air: A literature review. *Atmos. Environ.* **2009**, *43*, 2229-2246, DOI: <https://doi.org/10.1016/j.atmosenv.2009.01.034>.

(13) Lin, S.H.; Juang, R.S. Adsorption of phenol and its derivatives from water using synthetic resins and low-cost natural adsorbents: A review. *J. Environ. Manage.* **2009**, *90*, 1336-1349, DOI: <https://doi.org/10.1016/j.jenvman.2008.09.003>.

(14) Grabowska, E.; Reszczynska, J.; Zaleska, A. Mechanism of phenol photodegradation in the presence of pure and modified-TiO<sub>2</sub>: A review. *Water Res.* **2012**, *46*, 5453-5471, DOI: <https://doi.org/10.1016/j.watres.2012.07.048>.

(15) Colmenares, J.C. Sonication-induced pathways in the synthesis of light-active catalysts for photocatalytic oxidation of organic contaminants. *ChemSusChem* **2014**, *7*, 1512-1527, DOI: 10.1002/cssc.201402190.

(16) Sathishkumar, P.; Mangalaraja, R.V.; Anandan, S. Review on the recent improvements in sonochemical and combined sonochemical oxidation processes – A powerful tool for destruction of environmental contaminants. *Renew. Sust. Energ. Rev.* **2016**, *55*, 426-454, DOI: <https://doi.org/10.1016/j.rser.2015.10.139>.

(17) Colmenares, J.C.; Lisowski, P.; Łomot, D. A novel biomass-based support (Starbon) for TiO<sub>2</sub> hybrid photocatalysts: a versatile green tool for water purification. *RSC Adv.* **2013**, *3*, 20186-20192, DOI: 10.1039/C3RA43673J.

(18) Wang, G.; Cheng, B.; Zhang, J.; Xu, L.; Yin, T. Facile Synthesis and photocatalytic property of titania/carbon composite hollow microspheres with bimodal mesoporous shells. *Int. J. Photoenergy* **2012**, *9*, 1-9, DOI: 10.1155/2012/976389.

- (19) Coromelci-Pastravanu, C.; Ignat, M.; Popovici, E.; Harabagiu V. TiO<sub>2</sub>-coated mesoporous carbon: Conventional vs. microwave-annealing process. *J. Hazard. Mater.* **2014**, *278*, 382-390, DOI: <https://doi.org/10.1016/j.jhazmat.2014.06.036>.
- (20) Gregg, S.J.; Sing, K.S.W. Adsorption, Surface Area and Porosity, Academic Press. London, **1982**, DOI: 10.1002/bbpc.19820861019.
- (21) Xiong, L.B.; Li, J.L.; Yang, B.; Yu, Y. Ti<sup>3+</sup> in the surface of titanium dioxide: generation, properties and photocatalytic application. *J. Nanomater.* **2012**, *13*, 831524-831537, DOI: 10.1155/2012/831524.
- (22) Wong, C.P.P.; Lai, C.W.; Lee, K.M.; Hamid, S.B.A. Advanced chemical reduction of reduced graphene oxide and its photocatalytic activity in degrading reactive black 5. *Materials* **2015**, *8*, 7118-7128, DOI: 10.3390/ma8105363.
- (23) Erjavec, B.; Kaplan, R.; Pintar, A. Effects of heat and peroxide treatment on photocatalytic activity of titanate nanotubes. *Catal. Today* **2015**, *241*, 15-24, DOI: <https://doi.org/10.1016/j.cattod.2014.04.005>.
- (24) Kim, C.H.; Kim, B.H.; Yang, K.S. TiO<sub>2</sub> nanoparticles loaded on graphene/carbon composite nanofibers by electrospinning for increased photocatalysis. *Carbon* **2012**, *50*, 2472-2481, DOI: <https://doi.org/10.1016/j.carbon.2012.01.069>.
- (25) Pan, X.; Yang, M.Q.; Fu, X.; Zhang, N.; Xu, Y.J. Defective TiO<sub>2</sub> with oxygen vacancies: synthesis, properties and photocatalytic applications. *Nanoscale* **2013**, *5*, 3601-3614, DOI: 10.1039/C3NR00476G.
- (26) Park, D.R.; Zhang, J.; Ikeue, K.; Yamashita, H.; Anpo, M. Photocatalytic oxidation of ethylene to CO<sub>2</sub> and H<sub>2</sub>O on ultrafine powdered TiO<sub>2</sub> photocatalysts in the presence of O<sub>2</sub> and H<sub>2</sub>O. *J. Catal.* **1999**, *185*, 114-119, DOI: <https://doi.org/10.1006/jcat.1999.2472>.
- (27) Suriye, K. Praserttham, P., Jongsomjit, B. Control of Ti<sup>3+</sup> surface defect on TiO<sub>2</sub> nanocrystal using various calcination atmospheres as the first step for surface defect creation and its application in photocatalysis. *Appl. Surf. Sci.* **2007**, *253*, 3849-3855, DOI: <https://doi.org/10.1016/j.apsusc.2006.08.007>.
- (28) Hoffmann, M.R.; Martin, S.T.; Choi, W.; Bahnemann, D.W. Environmental applications of semiconductor photocatalysis. *Chem. Rev.* **1995**, *95*, 69-96, DOI: 10.1021/cr00033a004.
- (29) Luo, L.; Yang, Y.; Xiao, M.; Bian, L.; Yuan, B.; Liu, Y.; Jiang, F.; Pan, X. A novel biotemplated synthesis of TiO<sub>2</sub>/wood charcoal composites for synergistic removal of bisphenol A by adsorption and photocatalytic degradation. *Chem. Eng. J.* **2015**, *262*, 1275-1283, DOI: <https://doi.org/10.1016/j.cej.2014.10.087>.

- (30) Chen, C.; Long, M.; Zeng, H.; Cai, W.; Zhou, B.; Zhang, J.; Wu, Y.; Ding, D.; Wu, D. Preparation, characterization and visible-light activity of carbon modified TiO<sub>2</sub> with two kinds of carbonaceous species. *J. Mol. Catal. A: Chem.* **2009**, *314*, 35-41, DOI: <https://doi.org/10.1016/j.molcata.2009.08.014>.
- (31) Keiluweit, M.; Nico, P.S.; Johnson, M.G.; Kleber, M. Dynamic molecular structure of plant biomass-derived black carbon (biochar). *Environ. Sci. Technol.* **2010**, *44*, 1247-1253, DOI: 10.1021/es9031419.
- (32) Antonio-Cisneros, C.M.; Dávila-Jiménez, M.M.; Elizalde-González, M.P.; García-Díaz, E. TiO<sub>2</sub> immobilized on manihot carbon: optimal preparation and evaluation of its activity in the decomposition of indigo carmine. *Int. J. Mol. Sci.* **2015**, *16*, 1590-1612, DOI: 10.3390/ijms16011590.
- (33) Yu, S.; Yun, H. J.; Kim, Y. H.; Yi, J. Carbon-doped TiO<sub>2</sub> nanoparticles wrapped with nanographene as a high performance photocatalyst for phenol degradation under visible light irradiation. *Appl. Catal., B* **2014**, *144*, 893-899, DOI: <https://doi.org/10.1016/j.apcatb.2013.08.030>.
- (34) Fernández-Ibáñez, P.; Polo-López, M.I.; Malato, S.; Wadhwa, S.; Hamilton, J.W.J.; Dunlop, P.S.M.; D'Sa, R.; Magee, E.; O'Shea, K.; Dionysiou, D.D.; Byrne, J.A. Solar photocatalytic disinfection of water using titanium dioxide graphene composites. *Chem. Eng. J.* **2015**, *261*, 36-44, DOI: <https://doi.org/10.1016/j.cej.2014.06.089>.
- (35) Beams, R.; Cancado, L.G.; Novotny, L. Raman characterization of defects and dopants in graphene. *J. Phys.: Condens. Matter* **2015**, *27*, DOI: <https://doi.org/10.1088/0953-8984/27/8/083002>.
- (36) Vinoth, R.; Karthik, P.; Muthamizhchelvan, C.; Neppolian, B. Ashokkumar, M. Carrier separation and charge transport characteristics of reduced graphene oxide supported visible-light active photocatalysts. *Phys. Chem. Chem. Phys.* **2016**, *18*, 5179-5191, DOI: 10.1039/C5CP08041J.
- (37) Yu, Y.; Wen, W.; Qian, X.Y.; Liu, J.B.; Wu, J.M. UV and visible light photocatalytic activity of Au/TiO<sub>2</sub> nanoforests with Anatase/Rutile phase junctions and controlled Au locations. *Sci. Rep.* **2017**, *7*, 1-13, DOI: 10.1038/srep41253.
- (38) Wojcieszak, R.; Gaigneaux, E.M.; Ruiz, P. Direct methyl formate formation from methanol over supported palladium nanoparticles at low temperature. *ChemCatChem* **2013**, *5*, 339-348, DOI: 10.1002/cctc.201200325.

- (39) Chen, B.; Zhou, D.; Zhu, D. Transitional adsorption and partition of nonpolar and polar aromatic contaminants by biochars of pine needles with different pyrolytic temperatures. *Environ. Sci. Technol.* **2008**, *42*, 5137-5143, DOI: 10.1021/es8002684.
- (40) Geng, Q.; Cui, W. Adsorption and photocatalytic degradation of reactive brilliant red K-2BP by TiO<sub>2</sub>/AC in bubbling fluidized bed photocatalytic reactor. *Ind. Eng. Chem. Res.* **2010**, *49*, 11321-11330, DOI: 10.1021/ie101533x.
- (41) Pori, P.; Vilcnik, A.; Petri, M.; Skapin, A.S.; Mihelci, M.; Vuk, A.S.; Novak, U.; Orel, B. Structural studies of TiO<sub>2</sub>/wood coatings prepared by hydrothermal deposition of rutile particles from TiCl<sub>4</sub> aqueous solutions on spruce (*Picea Abies*) wood. *Appl. Surf. Sci.* **2016**, *372*, 125-138, DOI: <https://doi.org/10.1016/j.apsusc.2016.03.065>.
- (42) Kaichev, V.V.; Popova, G.Y.; Chesalov, A.; Saraev, A.A.; Zemlyanov, D.Y.; Beloshapkin, S.A.; Knop-Gericke, A.; Schlögl, R.; Andrushkevich, T.V.; Bukhtiyarov, V.I. Selective oxidation of methanol to form dimethoxymethane and methyl formate over a monolayer V<sub>2</sub>O<sub>5</sub>/TiO<sub>2</sub> catalyst. *J. Catal.* **2014**, *311*, 59-70, DOI: <https://doi.org/10.1016/j.jcat.2013.10.026>.
- (43) Liu, W.; Cai, J.; Ding, Z.; Li, Z. TiO<sub>2</sub>/RGO composite aerogels with controllable and continuously tunable surface wettability for varied aqueous photocatalysis. *Appl. Catal., B* **2015**, *174-175*, 421-426, DOI: <https://doi.org/10.1016/j.apcatb.2015.03.041>.
- (44) Fu, X.; Yang, H.; Sun, H.; Lu, G.; Wu, J. The multiple roles of ethylenediamine modification at TiO<sub>2</sub>/activated carbon in determining adsorption and visible-light-driven photoreduction of aqueous Cr(VI). *J. Alloys Compd.* **2016**, *662*, 165-172, DOI: <https://doi.org/10.1016/j.jallcom.2015.12.019>.
- (45) Omri, A.; Lambert, S.D.; Geens, J.; Bennour, F.; Benzina, M. Synthesis, surface characterization and photocatalytic activity of TiO<sub>2</sub> Supported on almond shell activated carbon. *J. Mater. Sci. Technol.* **2014**, *30*, 894-902, DOI: <https://doi.org/10.1016/j.jmst.2014.04.007>.
- (46) Kominami, H.; Sugahara, H.; Hashimoto, K. Photocatalytic selective oxidation of methanol to methyl formate in gas phase over titanium (IV) oxide in a flow-type reactor. *Catal. Commun.* **2010**, *11*, 426-429, DOI: <https://doi.org/10.1016/j.catcom.2009.11.014>.
- (47) Wojcieszak, R.; Karelovic, A.; Gaigneaux, E.M.; Ruiza, P. Oxidation of methanol to methyl formate over supported Pd nanoparticles: insights into the reaction mechanism at low temperature. *Catal. Sci. Technol.* **2014**, *4*, 3298-3305, DOI: 10.1039/C4CY00531G.
- (48) El-Roz, M.; Kus, M.; Cool, P.; Thibault-Starzyk, F. New operando IR technique to study the photocatalytic activity and selectivity of TiO<sub>2</sub> nanotubes in air purification: influence of



temperature, UV intensity, and VOC concentration. *J. Phys. Chem. C* **2012**, *116*, 13252-13263, DOI: 10.1021/jp3034819.

(49) Liu, L.; Luo, C.; Xiong, J.; Yang, Z.; Zhang, Y.; Cai, Y.; Gu, H. Reduced graphene oxide (rGO) decorated TiO<sub>2</sub> microspheres for visible-light photocatalytic reduction of Cr(VI). *J. Alloys Compd.* **2017**, *690*, 771-776, DOI: <https://doi.org/10.1016/j.jallcom.2016.08.197>.

(50) Zhang, Y.; Deng, S.; Sun, B.; Xiao, H.; Li, L.; Yang, G.; Hui, Q.; Wu, J. Preparation of TiO<sub>2</sub>-loaded activated carbon fiber hybrids and application in a pulsed discharge reactor for decomposition of methyl orange. *J. Colloid Interface Sci.* **2010**, *347*, 260-266, DOI: 10.1016/j.jcis.2010.03.064.

(51) Deka, B.K.; Maji, T.K. Effect of TiO<sub>2</sub> and nanoclay on the properties of wood polymer nanocomposite. *Composites Part A* **2011**, *42*, 2117-2125, DOI: <https://doi.org/10.1016/j.compositesa.2011.09.023>.

(52) Dong, F.; Wang, H.; Wu, Z. One-step “green” synthetic approach for mesoporous C-doped titanium dioxide with efficient visible light photocatalytic activity. *J. Phys. Chem. C* **2009**, *113*, 16717-16723, DOI: 10.1021/jp9049654.

(53) Liu, G.; Yan, X.; Chen, Z.; Wang, X.; Wang, L.; Lu, G.Q.; Cheng, H.M. Synthesis of rutile–anatase core–shell structured TiO<sub>2</sub> for photocatalysis. *J. Mater. Chem.* **2009**, *19*, 6590-6596, DOI: 10.1039/B902666E.

(54) Whiting, G.T.; Kondrat, S. A.; Hammond, C.; Dimitratos, N.; He, Q.; Morgan, D.J.; Dummer, N.F.; Bartley, J.K.; Kiely, C.J.; Taylor, S.H.; Hutchings, G.J. Methyl formate formation from methanol oxidation using supported gold–palladium nanoparticles. *ACS Catal.* **2015**, *5*, 637-644, DOI: 10.1021/cs501728r.

(55) Ferrari, A.C.; Robertson, J. Interpretation of Raman spectra of disordered and amorphous carbon. *Phys. Rev. B* **2000**, *61*, 14095-14107, DOI: <https://doi.org/10.1103/PhysRevB.61.14095>.

(56) Zhao, C.X.; Niu, C.Y.; Qin, Z.J.; Ren, X.Y.; Wang, J.T.; Cho, J.H.; Jia, Y. H<sub>18</sub> Carbon: A new metallic phase with sp<sup>2</sup>-sp<sup>3</sup> hybridized bonding network. *Sci. Rep.* **2016**, *6*, 21879-21888, DOI: 10.1038/srep21879.

(57) Cartwright, R.J.; Esconjauregui, S.; Weatherup, R.S.; Hardeman, D.; Guo, Y.; Wright, E.; Oakes, D.; Hofmann, S.; Robertson, J. The role of the sp<sup>2</sup>:sp<sup>3</sup> substrate content in carbon supported nanotube growth. *Carbon* **2014**, *75*, 327-334, DOI: <https://doi.org/10.1016/j.carbon.2014.04.011>.

(58) Kumar, A.; Patil, S.; Joshi, A.; Bhoraskar, V.; Datar, S.; Alegaonkar, P. Mixed phase, sp<sup>2</sup>-sp<sup>3</sup> bonded, and disordered few layer graphene-like nanocarbon: Synthesis and

characterizations. *Appl. Surf. Sci.* **2013**, *271*, 86-92, DOI: <https://doi.org/10.1016/j.apsusc.2013.01.097>.

(59) Han, C., Zhang, N., Xu, Y.J. Structural diversity of graphene materials and their multifarious roles in heterogeneous photocatalysis. *Nano Today* **2016**, *11*, 351-372, DOI: <https://doi.org/10.1016/j.nantod.2016.05.008>.

(60) Zhang, N., Yang, M.Q., Tang, Z.R., Xu, Y.J. Toward improving the graphene-semiconductor composite photoactivity via the addition of metal ions as generic interfacial mediator. *ACS Nano* **2014**, *8*, 623-633, DOI: 10.1021/nm405242t.

(61) Yang, M.Q., Xu, Y.J. Selective photoredox using graphene-based composite photocatalysts. *Phys. Chem. Chem. Phys.* **2013**, *15*, 19102-19118, DOI: 10.1039/C3CP53325E.

(62) Etacheri, V.; Di Valentin, C.; Schneider, J.; Bahnemann, D.; Pillai, S.C. Visible-light activation of TiO<sub>2</sub> photocatalysts: Advances in theory and experiments. *J. Photochem. Photobiol. C: Photochem. Rev.* **2015**, *25*, 1-29, DOI: <https://doi.org/10.1016/j.jphotochemrev.2015.08.003>.

(63) Diebold, U. The surface science of titanium dioxide. *Surf. Sci. Rep.* **2003**, *48*, 53-229, DOI: [https://doi.org/10.1016/S0167-5729\(02\)00100-0](https://doi.org/10.1016/S0167-5729(02)00100-0).

(64) Essam, T.; Amin, M.A.; Tayeb, O.E.; Mattiasson B.; Guieysse, B. Sequential photochemical–biological degradation of chlorophenols. *Chemosphere* **2007**, *66*, 2201-2209, DOI: <https://doi.org/10.1016/j.chemosphere.2006.08.036>.

(65) Millar, G.J.; Rochester, C.H.; Waugh, K.C. Infrared study of methyl formate and formaldehyde adsorption on reduced and oxidised silica-supported copper catalysts. *J. Chem. Soc. Faraday Trans.* **1991**, *87*, 2785-2793, DOI: 10.1039/FT9918702785.

(66) Xu, B.; Madix, R.J.; Friend, C.M. Predicting gold-mediated catalytic oxidative-coupling reactions from single crystal studies. *Acc. Chem. Res.* **2014**, *47*, 761-772, DOI: 10.1021/ar4002476.

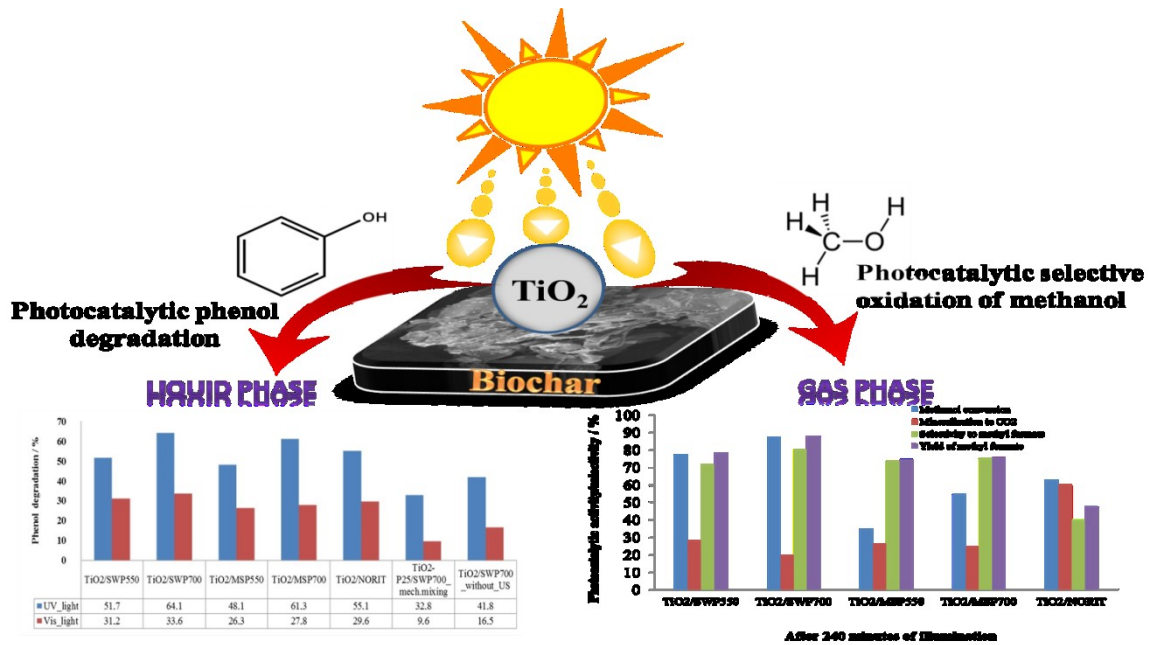
(67) Xu, B.; Haubrich, J.; Freyschlag, C.G.; Madix, R.J.; Friend, C.M. Oxygen-assisted cross-coupling of methanol with alkyl alcohols on metallic gold. *Chem. Sci.* **2010**, *1*, 310-314, DOI: 10.1039/C0SC00214C.

(68) Xu, B.; Liu, X.; Haubrich, J.; Friend, C.M. Vapour-phase gold-surface-mediated coupling of aldehydes with methanol. *Nat. Chem.* **2010**, *2*, 61-65, DOI: 10.1038/nchem.467.

(69) Yu, K.M.K.; Yeung, C.M.Y.; Tsang, S.C. Carbon dioxide fixation into chemicals (methyl formate) at high yields by surface coupling over a Pd/Cu/ZnO nanocatalysts. *J. Am. Chem. Soc.* **2007**, *129*, 6360-6361, DOI: 10.1021/ja0706302.

- (70) Tseng, T.K.; Lin, Y.S.; Chen, Y.J.; Chu H. A review of photocatalysts prepared by sol-gel method for VOCs removal. *Int. J. Mol. Sci.* **2010**, *11*, 2336-2361, DOI: 10.3390/ijms11062336.
- (71) Mo, D. Ye, D.Q. Surface study of composite photocatalyst based on plasma modified activated carbon fibers with TiO<sub>2</sub>. *Surf. Coat. Technol.* **2009**, *203*, 1154-1160, DOI: <https://doi.org/10.1016/j.surfcoat.2008.10.007>.
- (72) Fox, M.A.; Dulay, M.T. Heterogeneous photocatalysis. *Chem. Rev.* **1993**, *93*, 341-357, DOI: 10.1021/cr00017a016.
- (73) Linsebigler, A.L.; Lu, G.Q.; Yates, J.T. Photocatalysis on TiO<sub>2</sub> surfaces: principles, mechanisms, and selected results. *Chem. Rev.* **1995**, *95*, 735-758, DOI: 10.1021/cr00035a013.
- (74) Schwitzgebel, J.; Ekerdt, J.G.; Gerischer, H. Role of the oxygen molecule and of the photogenerated electron in TiO<sub>2</sub>-photocatalyzed air oxidation reactions. *J. Phys. Chem.* **1995**, *99*, 5633-5638, DOI: 10.1021/j100015a055.

## Graphical abstract



$\text{TiO}_2$ /biochar prepared via ultrasound assisted methodology and evaluated in liquid and gas phase; important contribution to the application of biomass-based materials and their utilization in photocatalytic processes.